

# **DC-DC Converter for PV Module Integration**

Estefanía Ruiz, Aitor Teran, Nicolai Fransen, Jesper Kloster,  
Thassilo Lang, Nicolás Murguizur Bustos

Energy Technology, INTRO-760, 2018-12

Master's Project



Copyright © Aalborg University 2018. All rights reserved.

This report has been written with L<sup>A</sup>T<sub>E</sub>X using TeXstudio. During the project PLECS, MATLAB and LTspice have been used for simulations, while the RT-box from Plexim has been used for implementation of the control system. The creation of flow charts have been done using [www.draw.io](http://www.draw.io). Hardware schematic and PCB layout have been created using Altium Designer.



**AALBORG UNIVERSITY**  
STUDENT REPORT

**Title:**

DC-DC Converter for PV Module Integration

**Theme:**

Dynamics in Electrical Energy Engineering

**Project Period:**

Fall Semester 2018

**Project Group:**

INTRO-760

**Participant(s):**

Estefanía Ruiz  
Aitor Teran  
Nicolai Fransen  
Jesper Kloster  
Nicolás Murguizur Bustos  
Thassilo Lang

**Supervisor(s):**

Lajos Török  
Dezso Sera

**Copies:** 1

**Page Numbers:** 72

**Date of Completion:**

December 6, 2018

*The content of this report is freely available, but publication (with reference) may only be pursued due to agreement with the author.*

**Department of Energy Technology**

Aalborg University

<http://www.aau.dk>

**Abstract:**

PV modules must work at their Maximum Power Point (MPP) to achieve the highest efficiency. Several environmental condition like partial shading can reduce the output power of the PV modules. Hence the goal of this project work is to design a Module Integrated Converter (MIC) in a PV module. A MIC consist on a DC-DC converter and a Maximum Power Point Tracking (MPPT) controller. It is decided to implement a non-inverting buck-boost converter with a Perturb and Observe (P&O) MPPT algorithm. The objective is that the PV module works at its MPP constantly regardless the environmental conditions.



# Contents

<b>Preface</b>	<b>ix</b>
<b>1 Introduction</b>	<b>1</b>
1.1 PV generation . . . . .	2
1.2 Module Integrated Conveter (MIC) . . . . .	3
1.3 Problem statement . . . . .	6
<b>2 State of the art</b>	<b>7</b>
2.1 Topologies of DC-DC converters . . . . .	7
2.1.1 Buck converter . . . . .	7
2.1.2 Boost converter . . . . .	8
2.1.3 Non-inverting buck-boost converter . . . . .	9
2.2 Maximum Power Point Tracking techniques . . . . .	11
2.2.1 Constant voltage . . . . .	11
2.2.2 Perturb and observe . . . . .	12
2.2.3 Incremental conductance . . . . .	13
<b>3 Non-inverting Buck-Boost converter design</b>	<b>15</b>
3.1 Selection of topology . . . . .	15
3.2 System requirements . . . . .	16
3.3 Component sizing . . . . .	17
3.4 Simulation Results . . . . .	18
<b>4 Hardware implementation</b>	<b>21</b>
4.1 Selection of commercial components . . . . .	21
4.1.1 Passive components . . . . .	21

4.1.2	Swithing circuitry . . . . .	22
4.1.3	Sensing circuitry . . . . .	28
4.1.4	Power Supplies . . . . .	34
4.2	PCB design . . . . .	34
4.2.1	PCB structure . . . . .	34
4.2.2	Design considerations . . . . .	35
4.2.3	Power Side . . . . .	36
4.2.4	Control Side . . . . .	37
<b>5</b>	<b>Maximum Power Point Tracking</b>	<b>39</b>
5.1	Perturb and Observe implementation . . . . .	39
5.2	Simulation of the MPPT . . . . .	44
5.2.1	Model of the PV panel . . . . .	44
5.2.2	Simulation results . . . . .	48
<b>6</b>	<b>Test and validation of results</b>	<b>55</b>
6.1	PCB building . . . . .	56
6.1.1	Power supplies . . . . .	56
6.1.2	Optocouplers . . . . .	56
6.1.3	Drivers . . . . .	57
6.1.4	Sensors . . . . .	57
6.2	MPPT . . . . .	58
6.2.1	RT-box . . . . .	58
6.2.2	PV simulator . . . . .	58
6.2.3	Load . . . . .	58
6.2.4	Experimental results . . . . .	58
<b>7</b>	<b>Discussion</b>	<b>59</b>
<b>8</b>	<b>Conclusion</b>	<b>61</b>
<b>Bibliography</b>		<b>63</b>
<b>A PCB schematics and Layout</b>		<b>67</b>

# Todo list

■ Supervisors: We are not sure if State of the Art is the right title of chapter 2.	7
■ For supervisors:	
Do you think it is worthed to justify why fets can have less losses than diodes? (that the losses on a transistor depend quadratically on the internal resistance and those on the diode depend linearly on the current)	
We were thinking that adding this justification might be a bit over the edge. . . . .	15
■ This figure will be updated. . . . .	20
■ Measure inductance behaviour at different currents. As the current component is getting too hot consider creating a new one. Complete inductor selection with final component. . . . .	22
■ Since you have made the simulations it would be a good idea to add them as appendices and refer to them. AT. Might be a good idea. Lets see if the limits of the document allows us (maximum number of pages). . . . .	23
■ This figure will be fixed. . . . .	28
■ If something should be deleted from P1 the output voltage sensor could be an option, NHF . . . . .	32
■ Make sure that the final frequency is not modified . . . . .	34
■ The unit of the temperature difference would be $K^{0.44}$ , but that doesn't looks really nice, what should we do? . . . . .	36
■ The tables will be resized to fit the page. . . . .	56
■ we will write here a little part about the iteration 1, which problem we have and how we fix it. . . . .	59



# Preface

This paper describes the report of the group project "DC-DC converter for PV module integration." It has been developed from the 10th of September to the 19th of December of 2018, at Aalborg University, Institute of Energy, by the group INTRO-760.

This document discusses the procedure and results of a DC to DC converter design to maximize the energy obtained from photovoltaic generation.

The literature references are shown in square brackets, with a number referring to a specific document which can be found in the bibliography. Pictures and tables will be denoted in the X,Y format, with X representing the chapter and Y the figure or table number. The process and development has been based on the Problem Based Learning (PBL) method.

Aalborg University, December 6, 2018

---

Estefanía Ruiz

eruiza18@student.aau.dk

---

Aitor Teran

ateran18@student.aau.dk

---

Nicolai Fransen

nfrans18@student.aau.dk

---

Jesper Kloster

jklost18@student.aau.dk

---

Thassilo Lang

tlang18@student.aau.dk

---

Nicolás Murguizur Bustos

nmurgu18@student.aau.dk



# Nomenclature

*Abbreviations:*

AC	Alternating Current
DC	Direct Current
FET	Field-Effect Transistor
IC	Integrated Circuit
MIC	Module Integrated Converter
MOSFET	Metal Oxide Semiconductor Field-Effect Transistor
MPP	Maximum Power Point
MPPT	Maximum Power Point Tracking
PBL	Problem Based Learning
PLECS	Piecewise Linear Electrical Circuit Simulation
PV	Photovoltaic
PWM	Pulse Width Modulation
SEPIC	Single Ended Primary Inductance Converter
STC	Standard Test Conditions
P&O	Perturb and Observe
LPF	Low Pass Filter

*Symbols:*

$\eta$	Efficiency
$^{\circ}\text{C}$	Degree Celsius
D	Duty Cycle
E	Energy
I	Current
$I_{mpp}$	MPP Current
$I_{out,max}$	Maximum output current
$I_{sc}$	Short Circuit Current
N	Number of PV Panels
P	Power
$P_{max}$	Maximum Power
t	Time
V	Voltage
$V_{ds}$	Drain Source Voltage
$V_{mpp}$	MPP Voltage
$V_{oc}$	Open Circuit Voltage
$V_{out,max}$	Maximum output voltage
$V_{out,min}$	Minimum output voltage
W	Watt
$W/m^2$	Irradiance

# 1

## Introduction

To this date, sustainable energy sources have become an area of worldwide focus in an attempt to reduce the environmental impact due to emissions of  $CO_2$  and other greenhouse gasses. The development of competitive systems to exploit renewable energy sources is the best alternative to reduce the use of fossil fuels for the production of electricity. Over the last years, there has been a considerable increase in electricity production from renewable energy sources being the fastest growing sectors wind and solar energy. In 2017, photovoltaic generation was the renewable energy source which experienced the highest increase in newly installed capacity. The total installed capacity reached approximately 402 GW[1].

Photovoltaic (PV) is referred to the production of electricity in the form of direct current (DC) directly from sunlight shining on solar cells. Solar cells are semiconductor devices which typically can produce around 0.5 V DC so they are connected to form a PV panel. These panels can also be connected to other PV panels resulting in a PV array [2]. This way, according to the system's requirements, the PV panels can be interconnected in series or parallel in order to get at the output a higher voltage or current, respectively.

Nevertheless, it is important to keep into consideration the mismatches that may appear on the power generated by the different PV panels. Mismatches can be caused by partial shading, manufacturing tolerances, defects in the PV modules due to weather conditions and ageing among others. Even a small mismatch can result in a high reduction of the power production from the entire PV array [3]. This will result in losses in the PV system which can be reduced by forcing every PV module to work at its Maximum Power Point (MPP) by using a Maximum Power Point (MPPT) unit. This can be reached by using electronic devices called MIC. MICs consist on DC-AC micro inverters or DC-DC converters that incorporate a MPPT control algorithm. The MPPT is used to ensure that the power generated is the one corresponding to the MPP of the PV module [3].

## 1.1 PV generation

The generation of direct current electricity from solar energy is a phenomenon known as *Photovoltaic effect* which was first discovered by a French physicist named Edmond Becquerel in 1839 [4]. This phenomenon allows the generation of electrical energy in a solar cell, when it is exposed to the sunlight [4]. The greater the intensity of the light (irradiance) that is absorbed by the PV panel, the higher the amount of electric power generated. On the other hand, the efficiency of the panel decreases with increasing temperature [2]. When the solar cell's temperature increases it results in a slightly increase of the generated current, however, the voltage decreases considerably [2]. This results in a reduction of the power generated by the solar panel.

Some of the most important parameters associated to a PV panel's data sheet are the following: maximum power ( $P_{max}$ ), open-circuit voltage ( $V_{oc}$ ), short-circuit current ( $I_{sc}$ ), MPP voltage ( $V_{mpp}$ ), MPP current ( $I_{mpp}$ ) and efficiency ( $\eta$ ) [2]. These features are important to define the characteristic curves of the PV panel. PV panel's I-V curves are a graphical representation of the relationship between the voltage and current of the solar panel. Different I-V curves are obtained for different temperatures and levels of irradiance [5]. Figure 1.1 shows the characteristic curves of a generic PV panel.

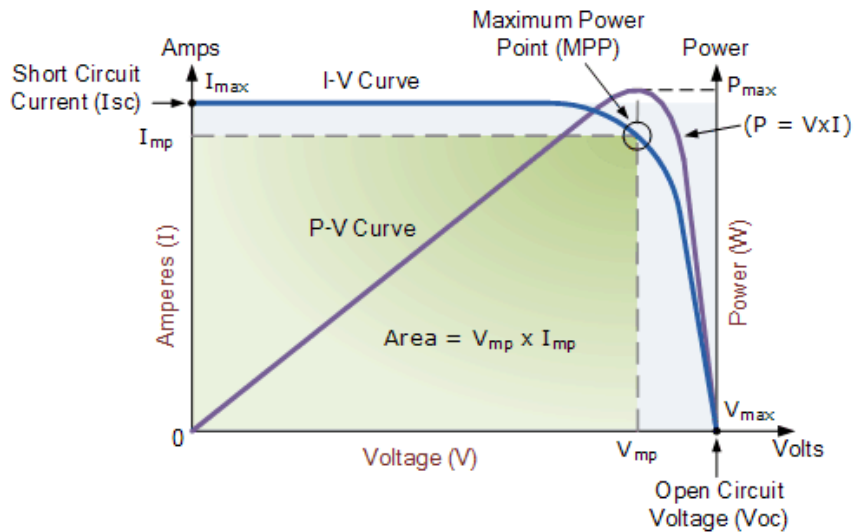
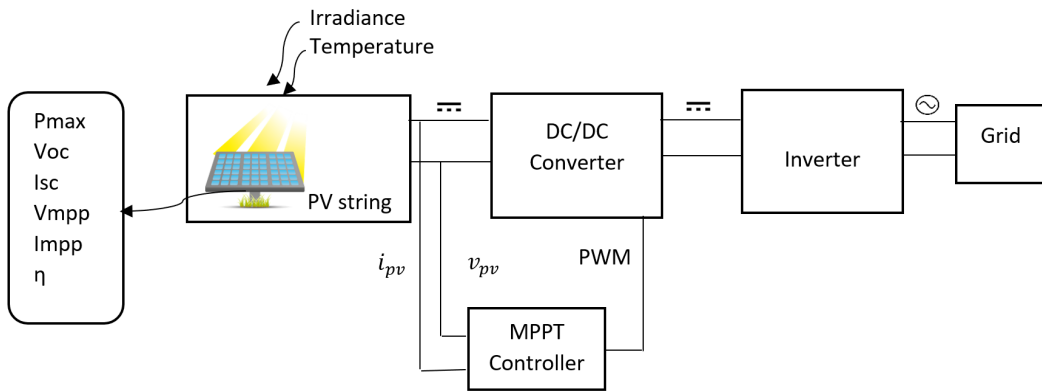


Figure 1.1: I-V and P-V curves of a generic solar panel [5].

The PV panel's I-V curve is shown in blue in Figure 1.1 for a given PV cell's temperature and solar irradiance. As it is well known, the power generated by a

PV cell is the product of current and voltage at each point. Hence, the P-V curve of the solar panel can be obtained and it is displayed in purple. From the P-V curve, the maximum power generated by the solar panel ( $P_{max}$ ) is obtained. This maximum power corresponds to the so called MPP and takes place for a specific combination of voltage ( $V_{mpp}$ ) and current ( $I_{mpp}$ ). Therefore, the ideal operating point of a PV panel corresponds to the MPP which varies according to the level of solar radiation and the temperature [2].

There are different types of photovoltaic systems, however, the most common PV systems implemented nowadays are grid-connected [2]. This type of PV system is mainly composed of a solar array, a DC-DC converter with an MPPT controller unit and an inverter, as shown in Figure 1.2.



**Figure 1.2:** Basic block diagram of a PV system.

As mentioned at the beginning of the chapter, PV modules can be connected to each other resulting in a PV array which generates electrical energy in the form of direct current. The MPPT controller unit takes the PV array's output voltage and current as input variables in order to calculate the corresponding duty cycle for tracking the MPP. The duty cycle is the input of a Pulse Width Modulation (PWM) block. The PWM is used to generate the pulses for the switching components of the DC-DC converter in order to get the PV array to work continuously at its MPP. The output of the DC-DC converter is connected to an inverter to convert the DC electric energy in an AC electrical signal compatible with the grid.

## 1.2 Module Integrated Conveter (MIC)

Usually, one MPPT is commonly used for many PV modules as shown in figure 1.2. This approach may lead to suboptimal efficiency of the system since the uneven power generated by the PV modules might lead to a system with a local MPP in addition to a global MPP [6]. In figure 1.3 a system exhibiting two MPP, due to

partial shading of one of the system's PV panels, is shown. In order to ensure that the system is working in the global MPP and not in the local MPP, the inverter's controller will have to perform a voltage sweep in order to find the global MPP. This voltage sweep is a higher level of complexity in the MPPT control system [6]. In any case, the system will not be able to get the maximum power generation, as one panel is bypassed by a diode.

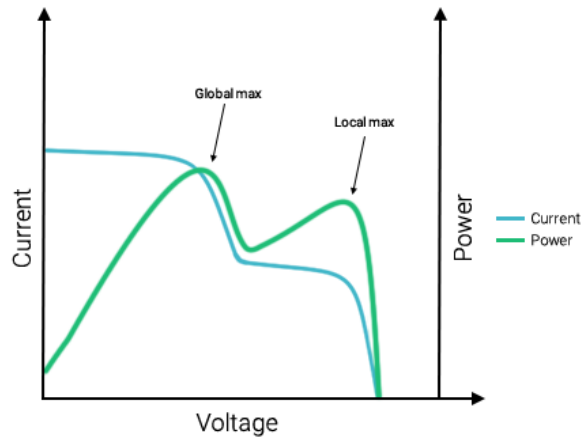


**Figure 1.3:** I-V curve of a system with more than one MPP [7].

Another approach is using a MIC. Which is a DC to DC converter featuring a MPPT controller included in each PV module which will result in higher overall efficiencies [8]. With this configuration, events like partial shading, uneven dirt, wear distribution or manufacturing imperfections are properly handled and do not affect the rest of the PV modules in the array. Also, a more detailed control of the plant is achieved since separate data from each individual panel is obtained [8]. Each PV module will then be connected directly to a MIC allowing the output voltage and current to be defined by the load. This way the system is able to operate at different voltage and current levels whilst maintaining the MPP [8].

MICs can be either microinverters or DC-DC converters. In figure 1.4 a PV system using MICs is used. Notice that  $N$  panels might be used. Series or parallel connections can be used to link MICs' outputs and then connect this output to the inverter input.

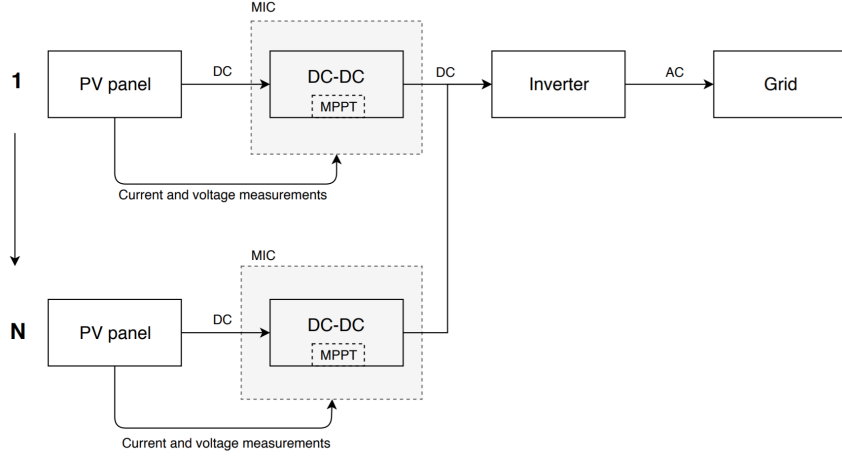


**Figure 1.4:** PV generation with DC-DC MIC system structure.

The panels with a MIC consisting on a microinverter, include a DC-DC converter with MPPT together with an inverter and are directly tied to grid. In figure 1.5 a microinverter system structure can be seen. For the user, this system is simpler, as only the PV must be purchase, the user does not have to worry about selecting and installing an inverter.

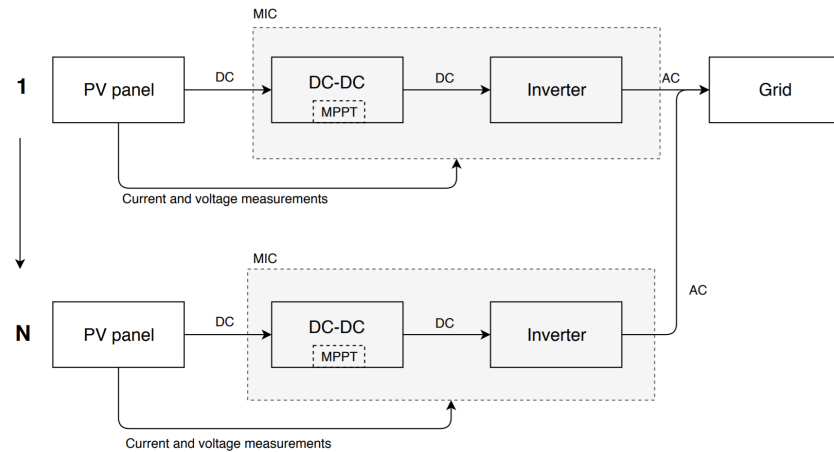


**Figure 1.5:** PV generation with microinverter MIC system structure.

The main advantage of the microinverter system is that it is simpler for the user, however, it implies an increase in costs and are usually less efficient than a DC-DC system with a single higher power inverter [8]. Therefore, for the development of this project a DC-DC MIC will be implemented.

### 1.3 Problem statement

The problem statement for this project can be formulated as the following question:

**How can a module integrated converter be designed to maximize the PV power generation under real conditions?**

The problem statement will be answered by fulfilling the following objectives:

- Design a DC-DC converter for integration with a PV panel.
- Analyze different implementations of MPPT techniques and implement the selected control system.
- Hardware implementation of the MIC components including PCB layout.
- Test of the system using a PV simulator and validation of the results.

# 2

## State of the art

The main topic for this project consist of the design of a MIC which basically is a DC-DC converter and a MPPT controller. Therefore this chapter analyzes different topologies for DC-DC converter commonly used in MICs. Also the chapter gives some background information of MPPT techniques.

Supervisors: We are not sure if State of the Art is the right title of chapter 2.

### 2.1 Topologies of DC-DC converters

#### 2.1.1 Buck converter

A buck converter is one of the simplest DC-DC converters with the task of decreasing the input voltage. The required components are a DC-source for the input voltage, two switches (a diode and a transistor), an inductor, a capacitor and a load. The equivalent diagram in figure 2.1 illustrates a buck converter.

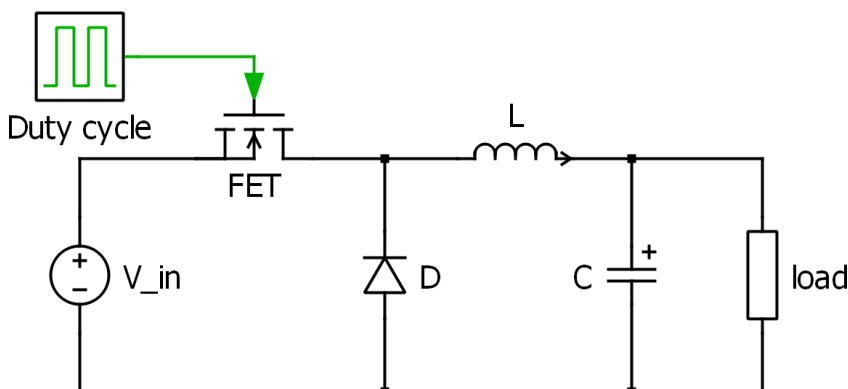


Figure 2.1: Equivalent circuit for the DC-DC buck converter.

A buck-converter performs in two operating states. During the first state, the MOSFET is conducting and the diode is working as an open-circuit, the voltage drop then is divided between the inductor and load. Since the voltage is split, the voltage drop on the load is lower than the one of the input source. In addition, both the capacitor and the inductor are being charged. In the second state, the MOSFET is switched off and the current flows through the diode. During this state, the inductor works as a current source and the capacitor stabilizes the voltage [9].

The main advantage for using the buck converter is that the structure is very simple and only one controlled switch is needed. Also, the component count and thus cost of components is low. Furthermore, the buck converter can reach efficiencies up to 99% [10].

However, this topology is not very versatile since it does not allow the increase of output voltage with respect to the input. Another drawback is the lack of galvanic isolation between the input and the output [11].

### 2.1.2 Boost converter

A boost converter is another type of DC-DC converter, it is similar to the buck but instead of lowering the output voltage, it produces a higher electrical potential at the output with respect to that at the input.

The circuit consists of two switches (a transistor and a diode), an inductor, a capacitor, a load and a DC-source for the input voltage. Figure 2.2 shows an equivalent circuit diagram with the aforementioned components.

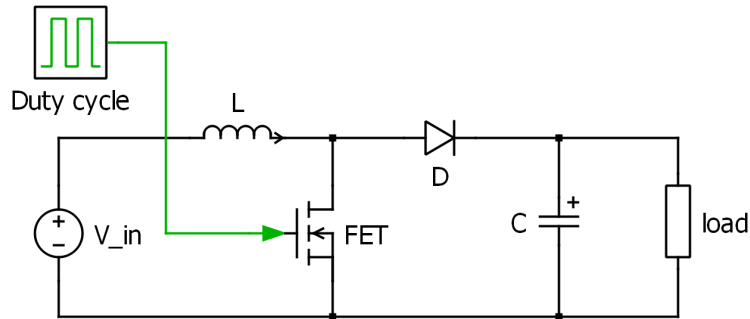


Figure 2.2: Equivalent circuit for the DC-DC boost converter.

Similarly to the buck converter, this topology has two states, when the MOSFET is on, the current flows only through the inductor because the diode is working as an open-circuit. Energy is then stored in the inductor, which voltage is equal to the input voltage, and current increases. Meanwhile, the capacitor releases the previously stored energy to the load. During the second state, the MOSFET is turned off, the current then loops through the inductor, diode, capacitor and the

load. Since the inductor had been previously charged, it now works as a current source in series with the voltage source of the circuit. The voltage across the load is then risen with respect to that at the input. Furthermore, the capacitor is charging [9].

An advantage for a boost converter is that it can raise the output voltage without using a transformer. It is also a cheap converter easy to control [11].

However, as it happened with the buck, the boost converter is also limited to rising the voltage and lowering it cannot be achieved. Also, if an error happens in the control of the MOSFET and it is left in ON-mode for a long time, a short-circuit is created and the current will increase until a component fails. Finally, this converter does not have galvanic isolation either.

### 2.1.3 Non-inverting buck-boost converter

The Non-inverting Buck-Boost converter is a DC to DC converter that allows the voltage at its output to be higher or lower than the voltage at its input. The topology can be seen in figure 2.3. It uses 4 switches, of which 2 are controlled devices.

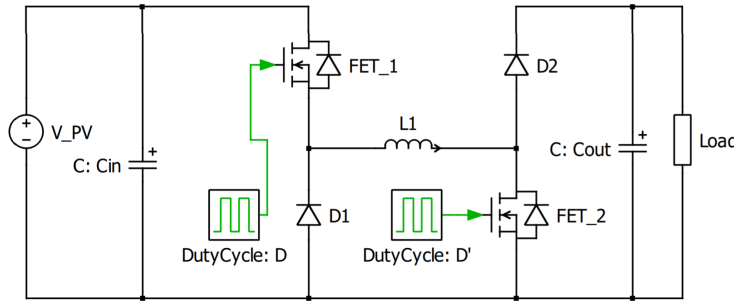


Figure 2.3: Non-inverting buck-boost converter.

The controller can force the system to work in any of the following modes:

1. Buck  $\rightarrow D \subset [0, 1]; D' = 0$
2. Boost  $\rightarrow D = 1; D' \subset [0, 1]$
3. Buck-Boost  $\rightarrow D \subset [0, 1]; D' \subset [0, 1]$

Usually the inverter's input voltage is fixed to some value higher than the grid's voltage. The possibility of higher and lower voltages at the converter's output allows different ways of associating photovoltaic modules. Then, the user is able to arbitrarily decide how many PV modules to link in series. Differently of what would happen in the case of Buck or Boost converters where the constraints regarding the number of panels are a bigger concern.

Compared with other topologies that can have both higher and lower voltages at the output, this DC-DC features a single inductor and no intermediate capacitor. With such reduction in passive components the price, efficiency and power density improves significantly [12].

One of the drawbacks of the non-inverting buck-boost topology is the control's complexity, which must calculate the appropriate duty cycle  $D$  and  $D'$  in any of the modes and also the transition between these modes. The buck-boost mode is specially complicated as there are two duty cycles to calculate. This problem might be addressed by setting a constant duty cycle in one of the bridge's legs and then the control will calculate the other leg's duty cycle [13].

Although this topology exhibits appropriate features, it can be further improved by replacing the diodes by MOSFETs. The circuit may be seen in figure 2.5, it's called Bidirectional Non-Inverting Buck-Boost converter. With this variation, the following changes occur:

1. The system becomes bidirectional.
2. The conduction losses are smaller.

If the system is bidirectional it can be used for different purposes, as the topology seen in figure 2.4, which features an isolated dc link. This topology needs a bidirectional MIC as energy flow in both directions is needed. It also allows diagnosis of PV modules.

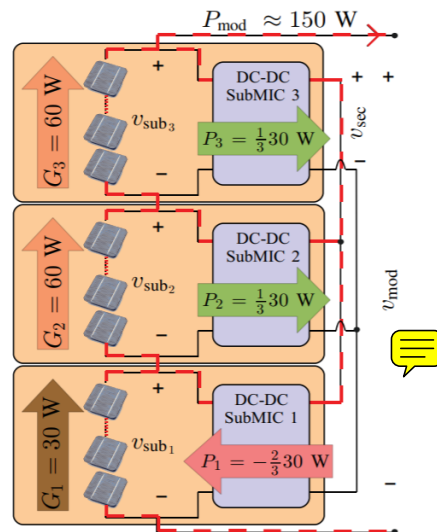


**Figure 2.4:** Bidirectional MIC use [8].

As seen in figure 2.5, notice that duty cycles of the switches that replace the diodes are  $\bar{D}$  and  $\bar{D}'$ . This line over the variables means that it is the complementary value of the original variable. The duty cycle is the boolean variable that indicates the conduction state of a switch.

Another drawback of the bidirectional system is the increased difficulty of the driver circuitry and the requirement of a dead time in order to avoid the short circuit of  $FET_1$  and  $FET_3$  or  $FET_2$  and  $FET_4$ , which could damage the system. When using diodes, the system is intrinsically protected against a shoot-through event.

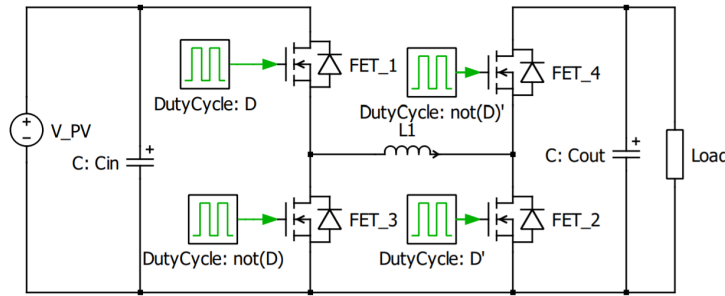


**Figure 2.5:** Bidirectional Non-inverting buck-boost converter.

## 2.2 Maximum Power Point Tracking techniques

There are a variety of different techniques for finding the maximum power point. Therefore only three different methods are used in this thesis, otherwise it would go beyond the scope of this work. These three methods are the perturb and observe, constant voltage and incremental conductance. Perturb and Observe (P&O) and incremental conductance are the most used algorithms in commercial PV panels. On the other hand, constant voltage has been selected as an idea for other less used methods. Each methods are described with a flow chart. Also there are mentioned the advantage and disadvantage from the methods.

### 2.2.1 Constant voltage

Empirical experiments have shown that the voltage of the MPP has a linear dependence on the open circuit voltage at different ambient conditions.

$$V_{MPP} = k \cdot V_{OC} \quad (2.1)$$

In the equation 2.1 k represents a constant that depends on the characteristics of the respective pv panel. To determine the value for k, the voltage for MPP and open

circuit must be recorded for each temperature and solar irradiation. According to different papers, this value lies between 70 and 80 percent of  $V_{OC}$ [14]. The algorithm starts with the recording of the open circuit voltage and a predetermined  $k$ -value. In each iteration step the  $V_{MPP}$  is calculated first. After this, the operating voltage is compared with the calculated voltage of the MPP. If the voltage is not equal, the constant  $k$  is changed for the next iteration step to reach the MPP. When the algorithm has reached the MPP, the algorithm is stopped, as you can see in the flowchart in the figure 2.6[15].

The advantage of using constant voltage is that only the voltage is measured and the system is controlled by a simple control loop. Therefore, implementation costs are low compared to the other two methods. The use of PV modules with the constant voltage as MPP algorithm is only possible in regions with low temperature fluctuations. The reason for this disadvantage is that the point of the MPP varies greatly with strong temperature fluctuations and the assumption of linear dependence is no longer valid. In addition, it is not possible to find the MPP with the algorithm if the PV module is partially shaded. Another disadvantage is the effort of calculating the optimal  $K$  for different irradiance and temperature is very high and therefore the complexity of the algorithm increase[15].

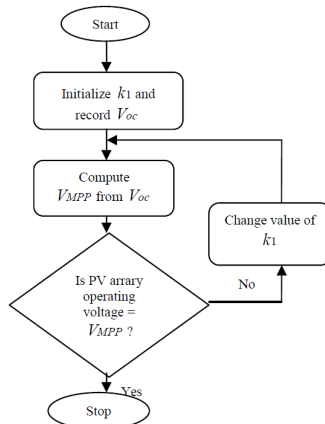


Figure 2.6: flow chart constant voltage[15].

### 2.2.2 Perturb and observe

With the method "perturb and observe", the currently measured power is periodically compared with the previous power. If the measured power is greater than the power from the previous measurement, the algorithm is moving in the right direction to the MPP. If a power reduction is detected after the comparison, the algorithm is moving away from the MPP. The next step is the identification of a voltage increase or reduction to regulate the voltage for getting the MPP voltage.

This depends on which side of the MPP the algorithm is working. If the algorithm detects less voltage than the MPP, the voltage for the next step should increase. If more voltage than the MPP is detected, the algorithm decreases the voltage for the next step to reach the MPP. The flowchart in the figure 2.7 illustrates this method. The classical algorithm uses a fixed step to change the voltage. When the MPP is reached, the algorithm oscillates around the MPP[15].

The required computing power of the P&O algorithm is also low, because it is easy to compute. The algorithm contains the calculation of the power and the comparison with previous power for each step. Another advantage of P&O is that a current sensor does not necessarily have to be used. There are scientific paper where only a voltage sensor is used [16]. There is a disadvantage when the algorithm is near to the MPP since, at this point, the algorithm oscillates around the MPP, so that the MPP cannot be reached exactly. The oscillation depends on the value of the fixed step. If the fixed step value is high, the MPP will be reached quickly. On the other hand, the oscillation around the MPP is high, which reduces the efficiency. The advantage of a small value is that the oscillation is small, but it takes more time to reach the MPP[6].

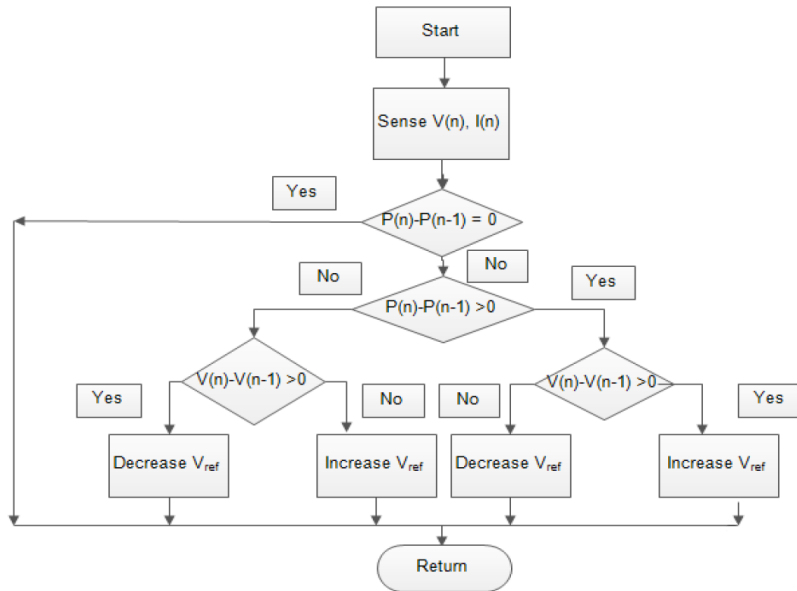


Figure 2.7: flow chart from perturb and observe[17].

### 2.2.3 Incremental conductance

The approach of incremental conductance is that the MPP is at the position where the derivative of the power with respect to the voltage is 0. On the left side of the

MPP the derivative is greater than 0 while on the right side it is less than 0, this behavior is described by the following equations.

$$\frac{dP}{dV} = 0, \text{ at MPP} \quad (2.2)$$

$$\frac{dP}{dV} > 0, \text{ left side from MPP} \quad (2.3)$$

$$\frac{dP}{dV} < 0, \text{ right side from MPP} \quad (2.4)$$

The algorithm compares the incremental conductance with the previous one to increase (left side of MPP) or decrease (right side of MPP) the voltage. After the MPP has been reached, the algorithm is stopped. Thus, there will be no oscillation around the MPP. If a change in the current is detected, the algorithm starts to find the MPP again, as you can see in the flowchart in the figure 2.8[6].

An advantage of incremental conductance is remaining exactly at the MPP that when this is reached. This increases the efficiency of the PV panel. As with perturb and observe, a fixed value is used to change the voltage. If the value is high, the probability is higher that the algorithm oscillated around the MPP. Two sensors are used for the implementation. In addition, the microcontroller requires a higher computing power than perturb and observe, since many more commands are called up during an iteration step. The costs for the algorithm development and microcontroller are higher compared to the other two algorithms[6].

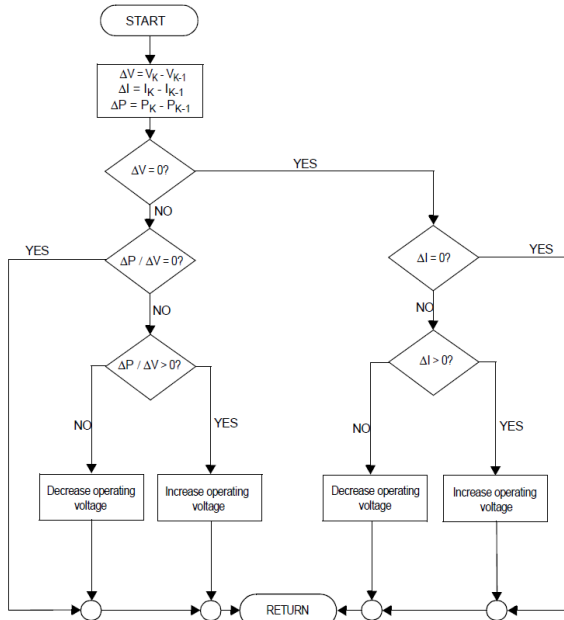


**Figure 2.8:** flow chart incremental conductance [6]

# 3

## Non-inverting Buck-Boost converter design

This chapter contains the initial analysis of the non-inverting buck-boost converter. The first part contains the selection of converter topology and the requirements which will be used during the design phase of the project. The second part includes the sizing of the passive components and the results of the open-loop simulation of the converter.

### 3.1 Selection of topology

The selection of converter topology is based on the research made in section 2.1. The converter should be able to allow both higher and lower output voltage compared to the input. This requirement will limit the buck and boost converters, which only convert either up or down. A buck-boost converter will therefore be implemented.

By using a 4 transistor buck-boost converter, instead of a 2 transistor, it is possible to further minimize the power loss since the losses on the transistor can be lower than those on the diodes.

For supervisors:

Do you think it is worthed to justify why fet's can have less losses than diodes? (that the losses on a transistor depend quadratically on the internal resistance and those on the diode depend linearly on the current)  
We were thinking that adding this justification might be a bit over the edge.

The 4 transistor buck-boost converter does also have the advantage of being bidirectional. This means that it is possible to extract current from the PV-module and also to inject current into the PV-module. When this happens, the PV-modules acts like a LED, radiating an infrared light when current is injected. If a PV-module is damaged has micro-cracks, the power generation will be affected. By injecting

current to the module it is much easier to find this small cracks, allowing the discovery of faulty modules before there is a drop in efficiency. This will increase the overall efficiency of the system and ease the maintenance sequence significantly.

The Bidirectional Non-Inverting Buck-Boost converter is chosen for these arguments. However the bidirectional functionality will not be addressed in this project, but could be a part of further development of the converter.

## 3.2 System requirements

For the design and test of the MIC it is of great importance to have the requirements of the system defined. The input requirements of the MIC will be based on the specifications of the PV panel *STP300S-24/Vd* from Suntech Power[18].

The specifications of the load of the MIC will be based on the commercial inverter "*Power-one STGU-105*"[19] in order to have the output voltage defined. From the inverter's datasheet it is found that the nominal voltage in the DC-link is 360V, with a maximum input power of 5500W. The development of this project will be based on these requirements because they are real commercial products that the user can purchase.

The maximum input power, voltage and current of the converter is decided by  $P_{max}$ ,  $V_{oc}$  and  $I_{sc}$  of the chosen PV-panel. The maximum output voltage is decided by the DC-link voltage and minimum string length, while the minimum output voltage is decided by the maximum string length. The maximum output current is decided by  $P_{max}$ , which ideally also will be the maximum output power, and the minimum output voltage. Table 3.1 shows the requirements of the MIC, extracted from the specifications of the PV panel and the inverter. It defines both the requirements regarding input, output and the length of PV panel strings.

<b>Input</b>	
Maximum input power ( $P_{max}$ )	300 [W]
Maximum input Voltage ( $V_{oc}$ )	45 [V]
Maximum input current ( $I_{sc}$ )	8.67 [A]
<b>Output</b>	
Maximum output voltage ( $V_{out,max}$ )	90 [V]
Minimum output voltage ( $V_{out,min}$ )	24 [V]
Maximum output current ( $I_{out,max}$ )	12.5 [A]
<b>PV system specification</b>	
Minimum string length	4
Maximum string length	15

Table 3.1: MIC requirements.

### 3.3 Component sizing

The power circuit includes three main passive components which are the inductor, the input capacitor ( $C_{in}$ ) and the output capacitor ( $C_{out}$ ). According to these values, the coil will influence the maximum current ripple that there will flow through it while the capacitors will set the voltage ripple at the input and at the output of the MIC. In order to calculate the minimal inductance and capacitance that components need to have, the worst case scenario was considered.

Therefore, in order to calculate these values the ripples have been set. For the current through the coil, a 10% maximum ripple has been chosen. The output capacitor will have a maximum of 0.5% voltage ripple. However, the input capacitor makes the PV-module output voltage flat, therefore the ripple found at  $C_{in}$  directly influences the maximum power extracted from the PV since it produces a deviation from the MPP. Giving this, a low input voltage ripple of 0.1% has been selected.

The ripple, however, also depends on the working frequency of the switches. In the case of this converter, such frequency has been set to 50kHz.

Since the coil ripple is a percentage of the absolute current, the worst case scenario for calculating it occurs when the current is lowest. A lower limit is then implemented at which the values will be calculated, this is the solar panel working at  $400W/m^2$  and at a temperature of  $25^\circ C$ .

Under this conditions, the MPP voltage obtained is  $V_{mpp} = 36.25V$  and the MPP current is  $I_{mpp} = 3.23A$ .

On the other hand, the capacitors will have a higher ripple when the current is maximum, this means that the system is working the maximum irradiance ( $1000W/m^2$ ).

The PV will then output a voltage of  $V_{mpp} = 36.9V$  and a current of  $I_{mpp} = 8.14A$ .

The minimum current flow through the coil is achieved when the boost mode is active. For this, the inductance is calculated for the maximum output voltage, which is when 4 MICs are connected in series. According to the equations stated in the section 2.2 of the book Fundamentals of Power Electronics [20], the inductance has been sized as seen in equation 3.1.

$$L = \frac{(V_{out} - V_{in}) \cdot D}{\Delta I_L \cdot f} = \frac{(90V - 36.25V) \cdot 0.4}{0.1 \cdot 3.23A \cdot 50kHz} = 1.3mH \quad (3.1)$$

On the other hand, the voltage used for  $C_{in}$  is obtained when buck mode is working with 15 MICs connected in series. This is a total output voltage of 24V. The capacitance required is then found as stated in equation 3.2 (Section 2.4 of Fundamentals of Power Electronics [20]).

$$C_{in} = \frac{I_{in} \cdot (1 - D)}{\Delta V_{in} \cdot f} = \frac{8.14A \cdot (1 - \frac{24V}{36.9V})}{0.001 \cdot 36.9V \cdot 50kHz} = 1.54mF \quad (3.2)$$

Finally,  $C_{out}$  is calculated in the worst case scenario of boost mode. The output voltage is then 90V. The values are calculated with the method found in section 2.3 of Fundamentals of Power Electronics [20]. The procedure can be seen in equation 3.3.

$$C_{out} = \frac{I_{out} \cdot D}{\Delta V_{out} \cdot f} = \frac{3.34A \cdot (1 - \frac{36.9V}{90V})}{0.005 \cdot 90V \cdot 50kHz} = 88\mu F \quad (3.3)$$

### 3.4 Simulation Results

To check that the calculations have been made correctly, an open loop simulation of the circuit was conducted. As it can be seen in figure 3.1 the circuit consists of the 4 MOSFETs, the inductor, the 2 capacitors and a load. The MOSFETs are controlled with two duty cycles  $D_1$  and  $D_2$ . FET1 and FET4 will get the actual duty cycle while FET2 and FET3 uses the inverted duty cycles. With the scope the output voltage and current through the inductor can be visualized.

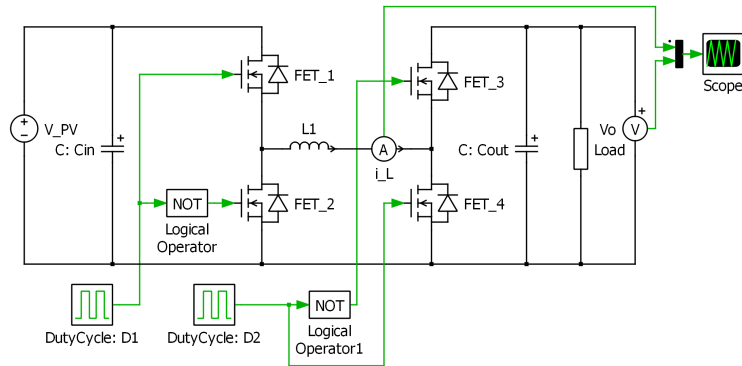
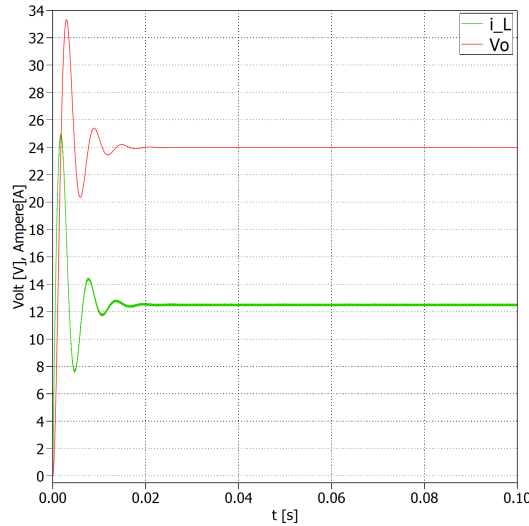


Figure 3.1: Ideal open loop simulation

The values for the components are  $C_{in} = 1880\mu F$ ,  $C_{out} = 820\mu F$  and  $L1 = 1mH$  as described earlier and  $V_{in} = 36.9V$ . At first the buck mode is simulated. In this mode  $D_2$  is 0. This means that FET4 is off and FET3 is on. The duty cycle for  $D_1$  is fixed at 0.65 which was calculated in ???. This should give an output voltage of 24V which can be seen in figure 3.2. The load is  $1.92\Omega$  because it produces 300W with an output voltage at 24V.



**Figure 3.2:** open loop simulation of buck mode

In buck mode the current through the inductor should be equal to the output current which with a load of  $1.92\Omega$  should be:

$$I_{out} = \frac{V_{out}}{R_{load}} = \frac{24V}{1.92\Omega} = 12.5A \quad (3.4)$$

To simulate the boost mode the input voltage is the same. Here the duty cycle for D2 is 0.638. This should respond to an output voltage of 90V and calculated with the same equation as . D1 is fixed to 1 so that FET1 is on and FET2 is off. This should give an output voltage of 90V. With 90V the output current should be 9A and then the current through the inductor is calculated like this:

$$I_L = \frac{1}{1 - 0.638} \cdot 12.5A = 9.207A \quad (3.5)$$

In figure 3.3 steady state the red line is again the output voltage which is the expected 90V just as the green line which is the current through the inductor is a bit more than 9A.

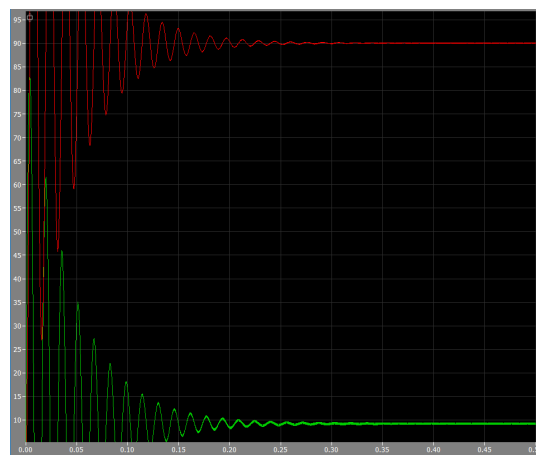


Figure 3.3: open loop simulation of boost mode

This figure will be updated.

# 4

## Hardware implementation

This chapter contains the hardware implementation of the non-inverting buck-boost converter. This mainly consists of the selection of commercial components, including switches, drivers, sensors, passive components etc. Additional circuits will also be designed to support the selected components. For the switch selection, power loss and temperature dissipation will be considered. This chapter also includes creation of the schematics and the PCB layout for the entire hardware implementation.

### 4.1 Selection of commercial components

#### 4.1.1 Passive components

Passive components includes input and output capacitors and inductor. The needed values were calculated in section 3.3. However, no tolerance or safety margin are included in those calculations. By the nature of the project, the goal is not to optimize price or size, but to validate the technical feasibility of the PV power optimizer. For this reason, the commercial input and output capacitors chosen has been oversized with the goal of easing the control task. In further work, optimization of this values should be performed.

The necessary input capacitance is  $1540\mu F$ . A safety margin of 20% has been applied resulting in a necessary input capacitance of  $1850\mu F$ . In order to achieve this value, 4 capacitors have been associated in parallel. The goal of paralleling the components is to decrease the parasitic inductance and resistance and ease the heat dissipation task. Four electrolytic capacitors of  $470\mu F$  [22] are placed in parallel to get a summed capacitance of  $1.880\mu F$ . The rating for these is 100V. The capacitors perform well in the working frequency and have low parasitic values, according to the data sheet [22].

For the output capacitor a  $820\mu F$  has been used [21].

Both for the input and output a  $100nF$  and a  $1\mu F$  capacitors are placed in parallel. These capacitors are SMD technology which have intrinsically low parasitic components. The goal is to support the higher capacitance capacitors during high frequency current peaks.

The calculated inductance is  $1.3mH$ .

Measure inductance behaviour at different currents. As the current component is getting too hot consider creating a new one. Complete inductor selection with final component.

#### 4.1.2 Switching circuitry

##### Switch sizing

The system must regulate the power flow in order to maximize the power generation. In order to achieve this, the system includes switches that control the current flow. The switches consist on MOSFET devices. The switching frequency of the system is 50 kHz. Although the market has IGBT which can switch at 50 kHz, MOSFET devices allow lower losses than IGBTs for system's current rating [23] [24].

The maximum output voltage of the system is 90V, however the voltage rating of the transistors was set to 150V in order to consider a safety margin, and thus, increase the reliability. The peak current through the transistors happens when the buck mode is active and the maximum number of MICs are used in series. The peak current is equal to 14 A. In order to reduce the conduction losses and the heat sink size, a low on resistance is desired. This constraints were used when searching for the ideal component. The chosen device is the IPB200N15N3. It exhibits the features seen in table 4.1.

<b>Maximum ratings</b>	
Continuous $I_D$	40 [A]
$V_{GS}$	$\pm 20$ [V]
Power dissipation	150 [W]
$V_{DS}$	150 [V]
$R_{DSon}$	20 [ $m\Omega$ ]
<b>Other values of interest</b>	
Input capacitance	1820 [pF]
Package	D2PAK
$V_{th}$ ( $V_{GS} = 3V$ )	3 [V]
$V_{th}$ ( $V_{GS} = 36V$ )	4.7 [V]
$R_{Gate}$	2.4 [ $\Omega$ ]

**Table 4.1:** MOSFET figures of merit.  $T = 25$  °C [25].

### Heat sink sizing

The procedure followed for validating the heat sink might be seen at figure 4.1. If the total temperature increase is within switch's safe operating area, then the heat sink is providing enough heat dissipation.



**Figure 4.1:** Heat sink validation procedure.

The power dissipated in the switches is equal to the sum of the conduction losses and the switching losses. The conduction loss might be calculated as seen in equation 4.1.

$$P_{cond} = i(t)^2 \cdot R_{DS} \quad (4.1)$$

The switching losses depend upon the switching frequency and the transistor's manufacturing characteristics. In order to calculate the value, the MOSFET's SPICE model was obtained from the manufacturer's website. The next step was to perform the simulation of the system. The system was simulated in both Buck and Boost modes. Special attention was put into the dead-band between PWM signals of different switches, to avoid current shoot through. After simulating, the average power dissipation under steady state was calculated in both Buck and Boost modes. Within every mode, the simulation was performed under the most unfavorable conditions, this is: Buck's output is 24 V and Boost's output is 90 V. The results can be seen in table 4.3, column 1.

$R_{DS}$  varies mainly dependent on the temperature. The models found neglect the temperature difference. Then, in order to get an approximated value considering temperature, the procedure will be to calculate the total losses at constant temperature using the SPICE model and then add the additional conduction losses due to the increase of the resistance, as expressed by equation 4.2.

$$\bar{P} = \overline{P_{loss,T=K}} + \bar{i}(t)^2 \cdot \Delta R_{DS} \quad (4.2)$$

Now the junction temperature based on the power dissipation calculated using the SPICE model is calculated. The ambient temperature is set to 50 °C, which is considered a realistic scenario. The thermal circuit can be seen in figure 4.2. The next step is to choose a commercial heat sink. The constraints are thermal resistance, size and price. TDEX6015/TH was found. Its features might be found

Since you have made the simulations it would be a good idea to add them as appendices and refer to them. AT. Might be a good idea. Lets see if the limits of the document allows us (maximum number of pages).

in table 4.2. The switches temperature will be analysed in order to validate the heat sink. The analysis considers all the transistors as a single power source.

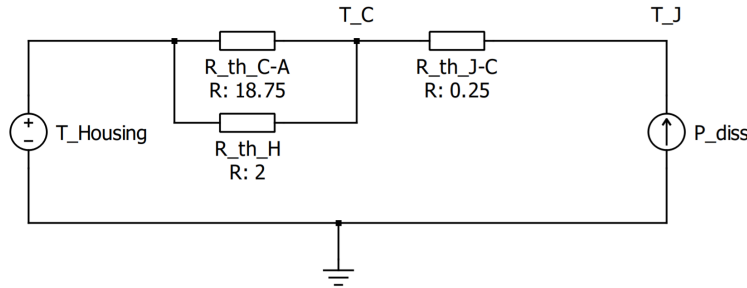


**Figure 4.2:** Thermal circuit used for sizing the heat sink

$$T_J = T_{housing} + \overline{P_{loss,T=K}} \cdot R_{thermal} \quad (4.3)$$

If no heat sink were used, according to equation 4.3, the junction temperature would become too high and the components would be damaged. See equation 4.4. This is mainly explained due to the fact that the thermal resistance between junction and ambient of the transistor is as high as  $75 \text{ }^{\circ}\text{C}/W$ .

$$T_J = 50 \text{ }^{\circ}\text{C} + 5.54W \cdot 75 \frac{\text{ }^{\circ}\text{C}}{W} = 465.5 \text{ }^{\circ}\text{C} \quad (4.4)$$

Features	
Size	60x60x16 [mm]
Thermal resistance	2.06 [K/W]

**Table 4.2:** Heat sink figures of merit [26].

$$T_J = 50 \text{ }^{\circ}\text{C} + 5.54W \cdot 2.06 \frac{\text{ }^{\circ}\text{C}}{W} = 61.41 \text{ }^{\circ}\text{C} \quad (4.5)$$

The Drain to Source resistance increase is calculated as explained in equation 4.6. The resistance difference is relatively small. The resistor at every temperature was collected from the component data sheet.

$$\Delta R_{DS} = |R_{DS,T=20 \text{ }^{\circ}\text{C}} - R_{DS,T=61.41 \text{ }^{\circ}\text{C}}| = 4 \text{ m}\Omega \quad (4.6)$$

The full power dissipation values can be found on table 4.3. To achieve an exact result, an iterative process should be followed. However, after the first iteration, the change ratio is extremely small and then, neglected. Now that the power dissipation has been calculated, the junction temperature must be checked in order to confirm that the heat sink has been properly sized. Equation 4.3 is used,

Switches power dissipation			
Switch	$\overline{P}_{loss,T=K}$ [W]	$i(t)^2 \cdot \Delta R_{DS}$ [W]	Total [W]
Buck mode			
M1	2.91	0.39	<b>3.30</b>
M2	0.82	0.21	<b>1.03</b>
M3	1.81	0.58	<b>2.39</b>
M4	0	0	<b>0</b>
<b>Total</b>	5.54	1.18	<b>6.72</b>
Boost mode			
M1	0.69	0.28	<b>0.97</b>
M2	0	0	<b>0</b>
M3	0.48	0.12	<b>0.6</b>
M4	3.31	0.18	<b>3.49</b>
<b>Total</b>	4.48	0.58	<b>5.06</b>

**Table 4.3:** Power dissipation analysis. Column 1, average power dissipation at constant 25 °C temperature. Column 2, extra power dissipation due to the increase of temperature.

substitution of values leads to 4.7. The difference is fairly small and the junction temperature remains within safe area. Then, TDEX6015/TH has been validated as a proper heat sink.

$$T_J = 50^\circ\text{C} + 6.72W \cdot 2.06 \frac{^\circ\text{C}}{\text{W}} = 63.84^\circ\text{C} \quad (4.7)$$

### Drivers and optocouplers

The control signal is generated by the control platform, which consists on a Plexim RTbox. In order to provide galvanic isolation between the converter and the control signal generator, optocouplers are used. The chosen optocoupler is the ACPL-P302. This optocoupler includes output signal circuitry which allows saving a pull-up or pull-down resistor. The IC is not an open collector device. Its main features might be seen at 4.4.

Maximum ratings	
Supply voltage	35 [V]
Average input current	25 [mA]
Peak output current	0.4 [A]
Other values of interest	
Input forward voltage	1.5 [V]
Package	SSOIC6

**Table 4.4:** Optocoupler figures of merit [27].

The signal from the optocoupler has to be amplified in order to drive the switches. The driver provides voltage amplification and current capability. The chosen IC to perform the task is NCP81074B. Find in table 4.5 its main features.

<b>Maximum ratings</b>	
Supply voltage	24 [V]
Output current (pulse < 0.5 $\mu$ s)	10 [A]
Reverse current (pulse < 1 $\mu$ s)	10 [A]
Input signal voltage	-6 to 24 [V]
<b>Other values of interest</b>	
Output resistance	0.4 [ $\Omega$ ]
Package	SOIC8

**Table 4.5:** Driver figures of merit [28].

The MOSFET is a voltage controlled device, the relationship between  $V_{GS}$  and  $V_{th}$  sets the drain to source maximum current, as seen in figure 4.3.

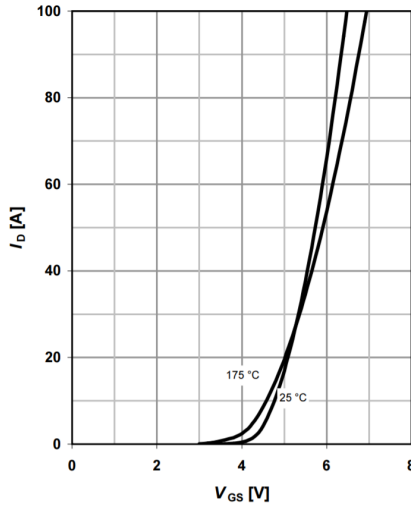


**Figure 4.3:** Drain to source current against gate to source voltage ( $V_{DS} > 2 \cdot I_D \cdot R_{DSon}$ ).

The dynamics of the switching can be modelled as a RC circuit, see figure 4.4. Both  $R_{driver\ out}$  and  $R_{MOSFET}$  are directly obtained from the components' data sheets,  $C_{iss}$  is also available in the MOSFET data sheet as input capacitance.

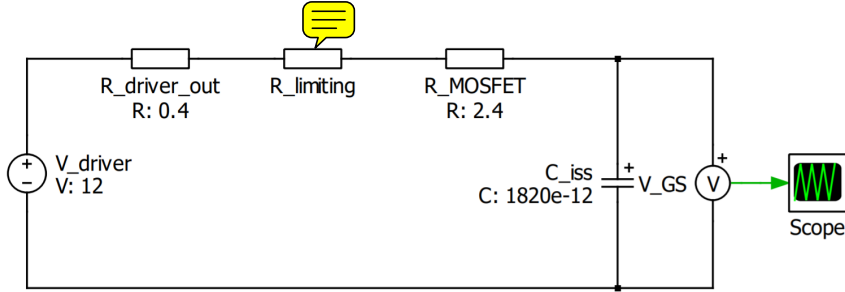


**Figure 4.4:** Simplified circuit used to model the MOSFET switching dynamics.

The time where the gate capacitor voltage reaches the threshold voltage produces a propagation delay from the driver output to the actual beginning of the MOSFET switching. In order to size the limiting resistor of the RC circuit, a time constraint was needed. This time constraint was arbitrarily set in relation with the switching frequency as described in equation 4.8. The 0.1% constraint results in a limiting resistor of  $20\ \Omega$ . The average power dissipation, according to simulation, is 13 mW. This value is well under the power rating of the used SMD resistor with 1206 package, which is 250 mW. However the peak power dissipation was also considered, as it is relatively high. According to simulation, the peak is equal to 5.4 W, see figure 4.5. Although this value exceeds the resistor power rating, some manufacturers agree that the peak power dissipation in pulses shorter than  $10\ \mu s$  using 1206 resistors is 19 W [29], [30]. Then the peak power dissipated shouldn't harm the component. Once the prototype is built, the thermal behaviour of the component is analysed with a thermal camera.

$$t_{delay} = t|_{V_{GS}=V_{th}} = \frac{T_{sw}}{1000} = 0.1\% \text{ of } T_{sw} = 20\ ns \quad (4.8)$$

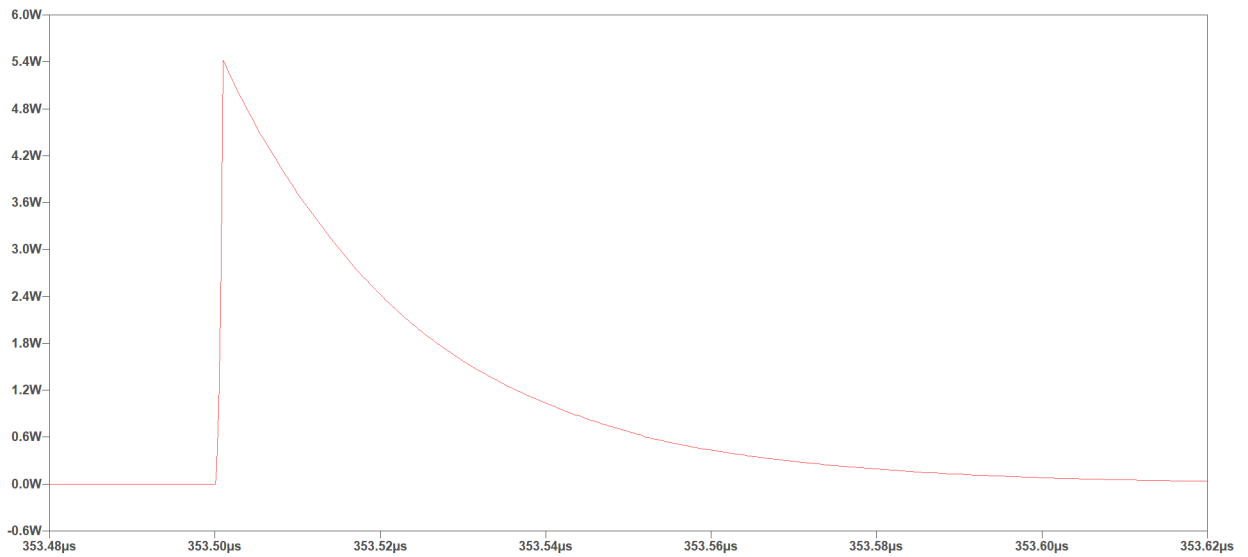


Figure 4.5: Detail of the power dissipated at  $R_{\text{limiting}}$  during MOSFET turn-on.

This figure will be fixed.

The implemented topology has the peculiarity that two MOSFETs' sources are not directly connected to ground. As explained previously, it is the Gate to Source voltage that determines whether the transistor is conducting or not. In order to get a floating voltage in the high side drivers, one option is to have isolated supplies for those drivers. The ground of this isolated supplies will be tied to the low side MOSFET's drain. More explanation regarding the isolated supplies might be found at 4.1.4.

In case that the drivers were damaged, the residual voltage of the transistor's gate might become undefined, then, in order to ensure that the switch is off, a pull down resistor is added between the gate and the source of the transistor. This resistor has been sized to  $1 \text{ M}\Omega$ , which discharges the gate voltage from 12 V to below its threshold in less than 3 ms.

### 4.1.3 Sensing circuitry

To implement the MPPT it's necessary to measure the output voltage and current of the PV-module. These measurements will be obtained by implementing a voltage and current sensor. A second voltage sensor will be implemented to measure the output voltage of the DC/DC converter, for possible future use.

To protect the RT-Box, it has been chosen to fully isolate it from the power stage of the converter. To do so, the sensors will have to include isolation between input and output.

### Input voltage sensor

The voltage sensor selected is the ACPL-C870 [31]. This sensor includes a optical isolation amplifier, which makes it well suited for isolated voltage sensing. Some relevant electrical specifications have been included in table 4.6. Figure 4.6 shows the placement of the two voltage sensors, where  $V_{in}$  and  $V_{out}$  are the input and output sensor respectively.

Recommended ratings		
Supply voltages	$V_{DD1}, V_{DD2}$	5 [V]
Input voltage range	$V_{in}$	0 – 2 [V]
Other values of interest		
Voltage gain	$G$	1 [V/V]
Output common-mode voltage	$V_{OCM}$	1.23 [V]
Gain tolerance	–	$\pm 3 [\%]$
Bandwidth	$BW$	100 [kHz]
Package	SSOP	[–]

Table 4.6: Electrical specifications ACPL-C870 [31].

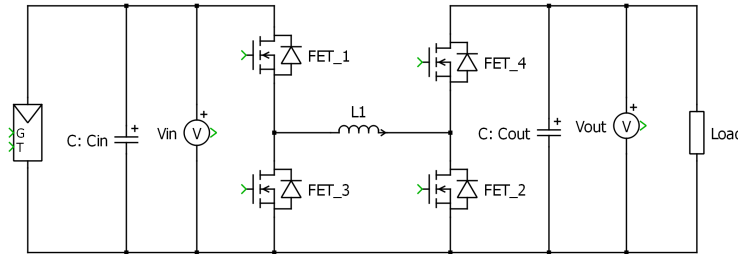


Figure 4.6: Voltage sensors placement.

**Voltage divider** The input voltage at the voltage sensor is recommended to be in the range of 0V – 2V. To divide the measured voltage into that range, a voltage divider will be implemented.

The maximum output voltage of the PV-module is the open-circuit voltage at 45.2V. To achieve a safety margin and to make the converter adaptable to other types of PV-modules, 50V has been selected. The current flow in the voltage divider has been set at 1mA, to secure a insignificant power loss. The resistors can be calculated with the following equations:

$$R_1 = \frac{V_{in,max} - V_{out}}{I} = \frac{50V - 2V}{1mA} = 48k\Omega \quad (4.9)$$

$$V_{out} = V_{in,max} \cdot \frac{R_2}{R_1 + R_2} \Rightarrow 2V = 50V \cdot \frac{R_2}{48k\Omega + R_2} \quad (4.10)$$

$$R_2 = 1.958k\Omega$$

To be able to select commercial resistors the values  $R_1 = 47k\Omega$  and  $R_2 = 2k\Omega$  have been chosen.

**Filtering** For a stable MPPT control, the measured voltage must have a very low ripple. To ensure this, a low-pass RC filter with a corner frequency at 50Hz, will be placed between the voltage divider and the sensor. The resistor of the filter will be  $R_1$  in the voltage divider. The capacitor will calculated as followed in equation 4.11:

$$C_{filter} = \frac{1}{2\pi \cdot f_c \cdot R_1} = \frac{1}{2\pi \cdot 50Hz \cdot 47k\Omega} = 67.7nF \quad (4.11)$$

To be able to select a commercial capacitor,  $C_{filter} = 68nF$  has been chosen.

**Amplification** The input range of the ADC in the RT-Box is 0V – 5V. To take advantage of the full range an amplifier will be implemented. The output of the voltage sensor is differential with an offset at 1.23V. Therefore a differential amplifier will be implemented using a LMC6484[32] quad operational amplifier. By using a quad amplifier, the same IC can be used for all the sensors. The relevant electrical specifications have been included in table 4.7.

Recommended ratings		
Supply voltage	$V_{DD}$	3 – 15.5 [V]
Input voltage range	$V_{in}$	$\pm V_{DD}$ [V]
Other values of interest		
Slew rate	$SR$	1.3 [V/ $\mu$ s]
Gain-Bandwidth product	$GBW$	1.5 [MHz]
Number of amplifiers	–	4 [-]
Package	–	SOIC [-]

**Table 4.7:** Electrical specifications LMC6484 [32].

The resistors of the differential amplifier will be sized with equation 4.12.

$$V_{out} = \frac{R_3}{R_1} \cdot (V_2 - V_1) \quad (4.12)$$

Where  $V_2 - V_1$  is the difference between the output pins of the voltage sensor. With unity gain in the voltage sensor, the maximum difference at the output will

be 2V. This should correspond to the maximum input voltage of the ADC at 5V.  $R_1$  is selected to be  $11k\Omega$ . The resistor  $R_3$  is now calculated using equation 4.12.

$$5V = \frac{R_3}{11k\Omega} \cdot 2V \quad (4.13)$$

$$R_3 = 27.5k\Omega$$

To be able to select commercial resistors the value of  $R_3$  it's rounded to be  $27k\Omega$ . Furthermore  $R_2 = R_1$  and  $R_4 = R_3$ , to get a balanced differential amplifier.

**The circuit** The circuit regarding the input voltage measurement is shown at figure 4.7.  $V_{in}$  is the measured voltage from the PV-module. The points  $OA1_+$  and  $OA1_-$  are connected to the non-inverting and inverting input of the amplifier respectively.  $OA1_{out}$  is connected to the output of the amplifier.  $C_{15}$  and  $C_{16}$  are decoupling capacitors for the two supply voltages. The maximum input voltage of the voltage sensor is 5V. Because of this a 4.7V zener diode has been added at the input, to protect it from over-voltage.

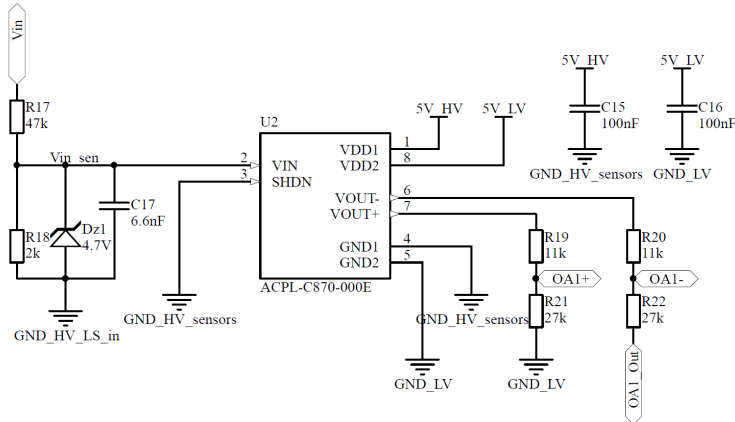


Figure 4.7: Input voltage sensor.

### Output voltage sensor

The voltage sensor at the output is design with the same procedure as the input sensor. The voltage divider will designed such that the values of the amplifier can be reused.

**Voltage divider** The maximum output voltage of the DC/DC converter will be 90V, when only 4 PV-modules are used. To insert a safety margin if one converter fails, the maximum sensed voltage will be designed at 120V.

The resistors will be sized by reusing equation 4.9 and 4.10.

$$R_1 = \frac{V_{in,max} - V_{out}}{I} = \frac{120V - 2V}{1mA} = 118k\Omega \quad (4.14)$$

$$V_{out} = V_{in,max} \cdot \frac{R_2}{R_1 + R_2} \Rightarrow 2V = 120V \cdot \frac{R_2}{118k\Omega + R_2} \quad (4.15)$$

$$R_2 = 2.03k\Omega$$

To be able to select commercial resistors  $R_{26} = 120k\Omega$  and  $R_{27} = 2k\Omega$  have been chosen.

**Filtering** The filter will be design with the same corner frequency at 50Hz, as for the input sensor.

The resistor of the filter will be  $R_1$  in the voltage divider. The capacitor will be calculated as followed in equation 4.16:

$$C_{filter} = \frac{1}{2\pi \cdot f_c \cdot R_1} = \frac{1}{2\pi \cdot 50Hz \cdot 120k\Omega} = 26.5nF \quad (4.16)$$

To be able to select a commercial capacitor  $C_{filter} = 33nF$  has been chosen. By using these values the actual corner frequency will be 40.2Hz.

**The circuit** The circuit regarding the input voltage measurement is shown at figure 4.8.

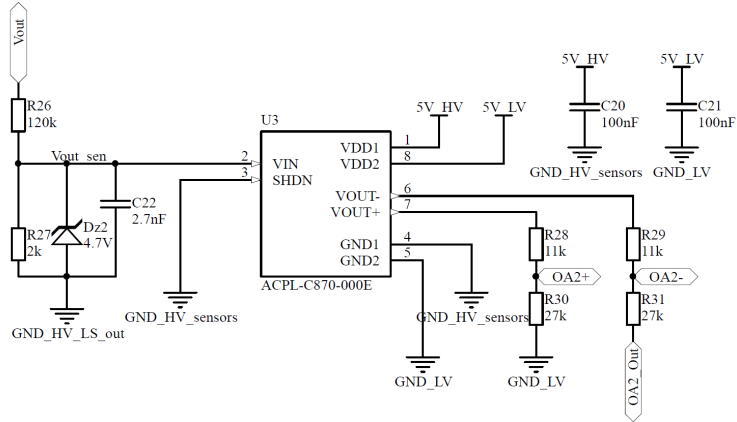
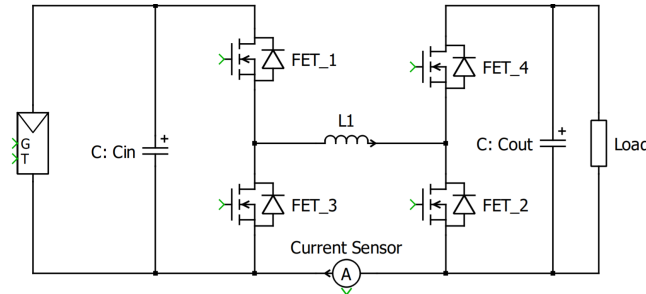


Figure 4.8: Output voltage sensor.

If something should be deleted from P1 the output voltage sensor could be an option, NHF

### Current sensor

The current along with the voltage of the PV allows the system to perform power calculation, which is needed for the MPPT algorithm. The current will be measured in series with the inductor with a hall effect sensor. Placing it in series with the PV module would be the easiest approach for MPPT, but placing it in parallel with the inductor allows implementing a current controller for possible future use.



**Figure 4.9:** Current sensor placement.

The sensor is a ACS723-20AB [33] which is a Hall effect sensor. Its features might be found in table 4.8 and its connection might be found in 4.10.

<b>Maximum ratings</b>	
Supply voltage	4.5-5.5 [V]
Gain	100 [mV/A]
Input range	$\pm 20$ [A]
<b>Other values of interest</b>	
Bandwidth	20 or 80 [kHz]
Package	SOIC8

**Table 4.8:** Current sensor figures of merit [33].

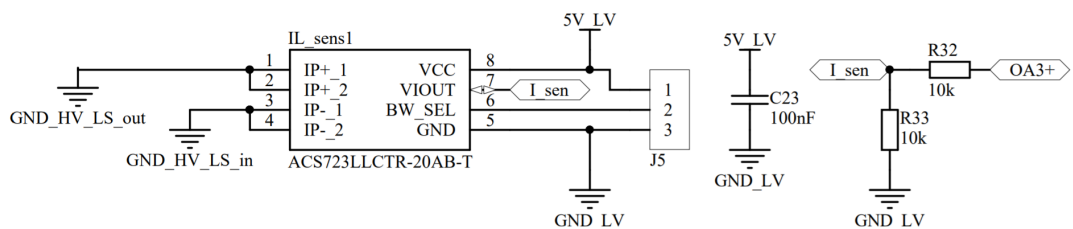


**Figure 4.10:** Current sensor connection.

The output of the sensor is a voltage proportional to the current following the next equation:

$$V_{current} = \frac{1}{10} i + 2.5 \quad (4.17)$$

In order to ease the task of the control, the signals are filtered by hardware. The current will be used by the MPPT, which frequency is 100Hz. The sensor output is filtered by a LPF which cut-off frequency is 50Hz. The cut-off frequency has been calculated by a thousandth of the switching frequency, which is 50kHz. Also the current might be used in the current controller, this signal will be filtered at 80kHz in order to remove high frequency noise, this cut-off frequency was selected as it is the sensor's bandwidth. The filters are first order low-pass filters implemented with a resistor in series with a capacitor.

Make sure that the final frequency is not modified

In order to calculate the current from the PV module, the converter working mode will have to be taken into account. Assuming continuous conduction mode, the average PV current is:

$$Buck \text{ mode} \rightarrow \overline{I_{in}} = \overline{i_{measured}} \cdot \delta \quad (4.18)$$

$$Boost \text{ mode} \rightarrow \overline{I_{in}} = \overline{i_{measured}} \quad (4.19)$$

$$Buck - Boost \text{ mode} \rightarrow \overline{I_{in}} = \overline{i_{measured}} \cdot \delta \quad (4.20)$$

#### 4.1.4 Power Supplies

In the first iteration of the converter, the drivers and the sensors will be supplied by an external 12V voltage source. This source will be used directly to supply the two lower leg MOSFET drivers. To support the higher leg drivers, two isolating 12V supplies will be used, with the external 12V as input. These will be two TRACO supplies TMA1212S [34]. The chosen voltage sensors need a 5V power supply at both input and output of the sensor. These should be isolated from each other. The input side will be supplied by a 5V voltage regulator, LD1117 [35], and the output side will be supplied by an external 5V source. The current sensor will also be supplied with 5V by the external voltage source. A LED will be added to every voltage source, to indicate if they are working.

## 4.2 PCB design

### 4.2.1 PCB structure

In order to proceed with the creation of the PCB, a schematic circuit has been designed. This compiles all the previously mentioned components as well as other components required for current limiting, decoupling, external connections, or

safety components for protection. Both PCB and schematic might be found in appendix A.

The schematic has been divided into four main sections, these are *main topology*, *power supplies*, *drivers* and *signal processing*.

The main topology includes the power circuit, this is the MOSFETs, the inductor, the input and output capacitors and the input and output connectors. It also includes discharging resistors for the capacitors which have been sized for one minute discharge time. The gate of the MOSFETs is also connected to the source through a resistor designed for 5ms discharge time. These safety resistors are implemented in order to ensure that the circuit is fully discharged when disconnected. Finally a series schottky diode is included at the input to protect the components in case of reverse connection, however, this diode can be short-circuited at any moment.

The power supplies include the 12V external input connector and two isolated commutative 12V. These two supplies are necessary to power the gates of the high side transistors and drivers. Lastly a 5V linear regulator supply has also been connected to feed the sensors. This 5V signal is referred to the power ground, thus the input 5V signal could not be used since it does not share the same ground.

The drivers section is composed of the isolating optocouplers and the MOSFET gate drivers, the PWM signals to the optocouplers come directly from the RT-box, meaning that a connector is also included here. Finally decoupling capacitors are added in the vicinity of the ICs in order to assure that the current peaks needed by these are granted.

The signal processing section is composed by the IC sensors and the operational amplifier. As stated previously, there are 2 isolated voltage sensors and a hall effect sensor for current measuring. Also, voltage dividers are located in this section, these include protection zener diodes limiting 5V output voltage and filtering capacitors, finally amplification resistors are added. The current sensor also includes a selection pin header which will allow different filtering frequencies options. The operational amplifier is also included.

Finally, test points have been added to the signals that might be measured.

### 4.2.2 Design considerations

Before starting the design of the PCB, some features were considered. First and most importantly, the power side is physically separated from the control side. This separation is done to reduce the electromagnetic coupling that the higher currents and voltages might induce in traces or ICs. A clear differentiation of the hot and cold sides of the PCB is seen in the layout. Also, test points have been located in the periphery of the PCB for easiest and safest testing. Current loops have been minimized as much as possible and ground planes are located across the PCB.

### 4.2.3 Power Side

One of the most important issues to take into consideration when designing the power traces of the converter has been the size of these. In order to allow a high flow of current through the traces while maintaining a relatively low temperature and a low impedance, the trace minimum width must be properly sized. For that goal a temperature constraint is needed. This constraint was arbitrarily set to 10 °C. Which will be the temperature increase of the traces working at full power. This constraint will lead to a high trace width, which is acceptable for a prototype. The calculation of the width has been performed following IPC-2221A section "6.2 Conductive Material Requirements" recommendations regarding trace width sizing. First, the needed cross sectional area of the trace must be calculated, as explained in equation 4.21.

$$A = \sqrt[0.725]{\frac{I}{0.048 \cdot \Delta T^{0.44}}} \quad (4.21)$$

$I$  stands for the current, and  $\Delta T$  is the temperature difference constraint. The highest average current will be used. See in equation 4.22 the result.

$$A = \sqrt[0.725]{\frac{12.5A}{0.048 \cdot 10^{0.44}}} = 530,9 \text{ mils}^2 \quad (4.22)$$

When the needed area is known, the width is calculated by dividing the area by the copper thickness. In our case, using 1oz PCB, the thickness is 35 $\mu\text{m}$ . See equation 4.23. It's necessary to perform unit conversion from  $\text{mils}^2$  to  $\text{mm}^2$ .

$$\text{Width} = \frac{A}{\text{Thickness}} = \frac{0.342\text{mm}^2}{0.035\text{mm}} = 9.78\text{mm} \quad (4.23)$$

Then 10 mm is set as trace minimum width.

The heat sink has conditioned the design of the power side of the PCB since most of the passive components do not fit underneath. The four MOSFETs are located at even distances and at the corners of the heat sink to allow the best possible dissipation. The drivers are also located very close to each one of the transistors to have the shortest path to the gate.

The coil has been cornered since it might induce high interference to other sensible devices. Especially the current sensor, which is hall-effect, has been located as far as possible from its influence. Also the ground plane has been removed from under the inductor in order to reduce interferences.

Finally, the high frequency capacitors are located very close to both power stages and the current loop area has been minimize to reduce the inductive behavior of this loop.

The unit of the temperature difference would be  $K^{0.44}$ , but that doesn't looks really nice, what should we do?

#### 4.2.4 Control Side

The control side has two different parts which are separated according to the ground that they have. On one side are located all the components that share the ground with the power side. This is the power supplies and the voltage dividers. The components that only have the low voltage ground, are located further away from the power circuit and finally some components act as bridges since they have both grounds. These components are the optocouplers and the voltage sensors, both with optical isolation.

This way, it is possible to separate the grounds at both sides reducing the possibility of having a short-circuit which may damage the control unit, in this case, the RT-box. However, the current sensor had to be located directly in the power side of the converter since the main current needs to flow through it. Since the current sensor shares the ground with the control unit, bigger clearances are included in all the traces coming from this sensor to reduce the possibility of short-circuit.

The test points located at the periphery break at some points this isolation clearance that was implemented in most parts of the circuit. However, since the test points are not carrying current and test points would always be removed in a final version of the PCB, this problem has not been considered.



# 5

## Maximum Power Point Tracking

This chapter contains the control of the non inverting buck-boost converter , so that the PV panel works at the maximum power point during operation. To achieve this, a MPPT algorithm is implemented. The selection of the MPPT algorithm is based on the knowledge from section 2.2 . Constant voltage is not applied in the project work. One of the requirements is that the algorithm can track the MPP despite changes in the environmental operation and this is not possible with an implementation of constant voltage. Since for the algorithm Incremental conductance the program needs more complex commands, the P&O algorithm was chosen because of the simpler implementation. At the beginning of the chapter the implemented algorithm is described with a flow chart. To validate the algorithm, a simulation of a non-inverting buck-boost converter with the MPPT algorithm is implemented using the software *PLECS*.

### 5.1 Perturb and Observe implementation

The basic operation of the P&O algorithm consists of perturbing the operating voltage of the PV module by means of the variation of the duty cycle of the DC-DC converter. After each perturbation the power generated by the PV module is measured (observed) and stored in order to compare it with the previous value of the power. Based on the result of the comparison the MPP can be tracked by deciding if in the next perturbation the panel's voltage should be increased or decreased.

There are different techniques for implement the P&O algorithm according to the value of the variable controlled by the MPPT and also depending if the perturb value is fixed or variable [36]. The conventional P&O algorithm uses a fixed perturb to generate a voltage or current reference signal for the outer control loop. The

outer loop is used to control the switching of the DC-DC converter. Another way of implementing the conventional P&O algorithm is using an adaptive perturb by setting the initial perturbation to 10% of the open-circuit voltage ( $V_{oc}$ ). After each iteration its value is decreased by 50% until it reaches 0.5% of  $V_{oc}$  [36]. A different technique consists on using the duty cycle of the converter as the variable controlled by the MPPT block. Therefore, it is not necessary to implement the outer control loop. This technique can also be implemented using fix or variable perturb step [36].

The P&O algorithm that will be implemented in this project is the MPPT controlling directly the duty cycle and using a variable perturb step. It was decided to directly control the duty cycle to simplify the control system. On the other hand, an adaptive perturb is selected instead of a fixed one. The reason is that the MPPT takes longer time to reach the MPP, if a small perturb step is implemented. However, using a large perturb step the tracking would be faster but the oscillations around the MPP would be higher [36]. For this reason, it was decided to start with a perturbation step of 10% of the  $V_{oc}$  until the system reaches a certain value close to the MPP. At this point the perturbation step is iteratively reduced to one third of its previous value in order to reach accurately the MPP with lower oscillations. Figure 5.1 shows the implementation of the system in PLECS including the MPPT which operates at a frequency of 100 Hz.

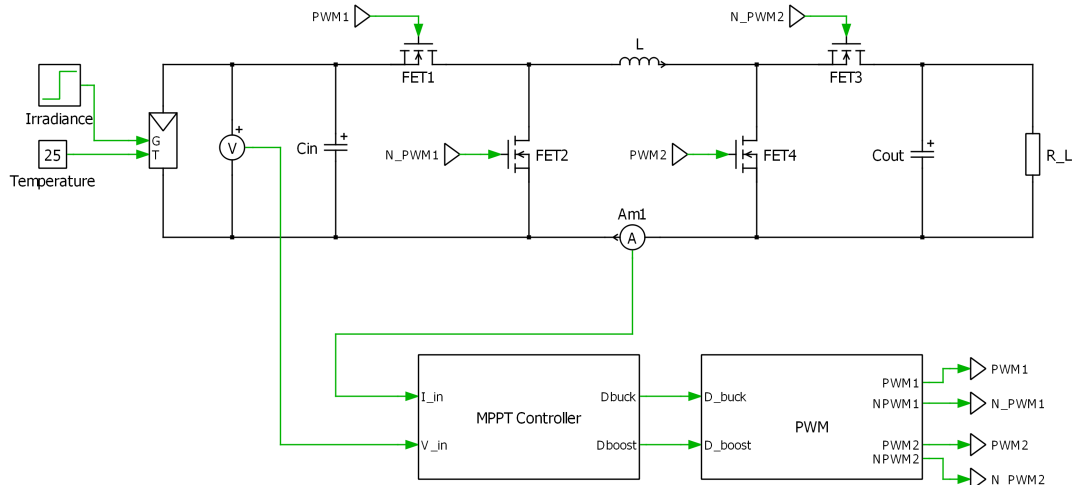


**Figure 5.1:** Block diagram of the system including the MPPT.

From the previous figure it is observed that the outputs of the MPPT block are the corresponding duty cycles for buck and boost mode. The perturb step is a control variable called *valg* which corresponds to the transfer function of the power converter. The transfer function when it is operating in buck and in boost mode is

shown in equations 5.1 and 5.2, respectively. The control variable  $valg$  will be used to increase or decrease the voltage from the PV panel. From the transfer function equations it is observed that when increasing  $valg$  then the voltage decreases and vice versa. Plotting this transfer functions and mapping them as shown in figure 5.2 it is possible to obtain the corresponding duty cycle for the buck or the boost mode. If the control variable from the MPPT is lower than 0.5 means that the output voltage is lower than the input voltage and thus the converter will work as a buck converter with duty cycle  $D_{buck} = 2 \cdot valg$ . On the other hand, if the control variable is  $valg \geq 0.5$  means that the output voltage is higher or equal than the input voltage and, therefore, the converter will operate in boost mode with duty cycle  $D_{boost} = 2 \cdot valg - 1$ . These duty cycles are used to generate the corresponding PWM signals according to the converter's mode of operation at each time.

$$\frac{V_o}{V_i} = D \quad (5.1)$$

$$\frac{V_o}{V_i} = \frac{1}{1 - D} \quad (5.2)$$

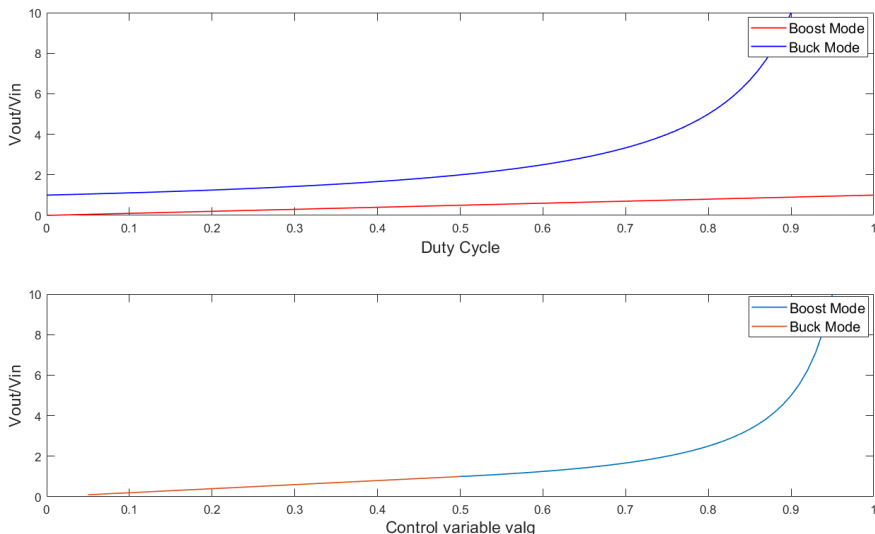


**Figure 5.2:** Mapping to decide the mode of operation.

The flow chart used for the implementation of the P&O algorithm is shown in figure 5.3. From the flow chart it can be observed that the MPPT is enabled when the panel's voltage has reached the value of the open-circuit voltage. The MPPT is forced to start at this point to be close to the value of the MPP. This means that the MPPT detects when the difference between the measured voltage and the previous voltage is lower than 0.1 then it starts the open loop calculation. This calculation

is done to make the MPPT faster because the algorithm starts with  $valg = 0$ . The open loop calculation decreases the voltage without evaluating the voltage and power. The condition for starting the MPPT evaluation is that  $counter = 15$  to ensure that the point of operation is closer to the MPP.

It is important to notice from figure 5.1 that the current measurement is carried out in the inductor instead of in the PV panel. This is done for possible future implementation of an outer control loop. For this reason, it is necessary to transform the measured current in order to get the corresponding measurement for the PV module's current. This current transformation is just necessary in the case of buck mode as explained in section 4.1.3. If the MPPT detects that the converter is working in buck mode, it multiplies the measured current by the corresponding duty cycle  $D_{buck} = 2 \cdot valg$ . In boost mode the average current through the inductor corresponds to the PV module's current.

The operation of the algorithm, shown in figure 5.3, is an iterative process. The PV panel's voltage and power, before and after applying a voltage perturbation, are compared in order to locate the point of operation. This way it is possible to decide if the panel's voltage has to be increased or decreased. Based on the PV characteristic curve shown in figure 1.1, the following situations can occur:

1. Increment of voltage and increment of power means that the point of operation is located to the left of the MPP. Therefore, the perturbation continues in the same direction (voltage is increased) with a fixed perturb step.
2. Increment of voltage and decrement of power means that the point of operation of the panel has gone from being located to the left of the MPP to the right of it. Therefore, the next perturbation is in the opposite direction (voltage is decreased) with a perturb step of one third of the previous step value.
3. Decrement of voltage and increment of power means that the operation point is located to the right of the MPP. Therefore, the perturbation continues in the same direction (voltage is decreased) with a fixed perturb step.
4. Decrement of voltage and decrement of power means that the point of operation of the panel has changed from being located to the right of the MPP to the left of it. Therefore, the next perturbation is in the opposite direction (voltage is increased) with a perturb step os one third of the previous step value.

After the process, once the MPP has been reached, the algorithm oscillates around this optimal point of operation. However in this case, as a variable perturb step is applied, the oscillations around the MPP will be much lower than using fixed perturb step.

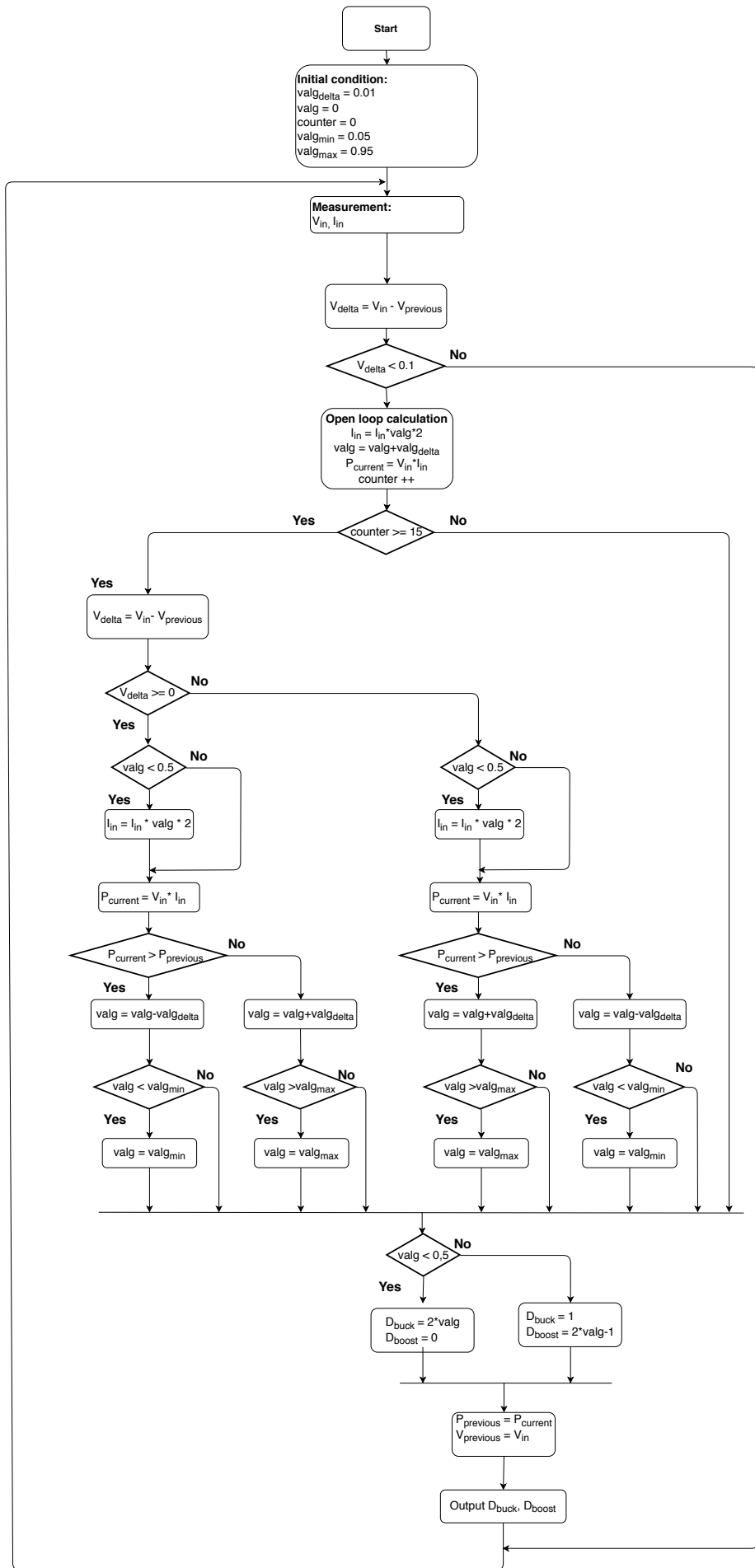


Figure 5.3: Flow chart for the Perturb &amp; Observe algorithm.

## 5.2 Simulation of the MPPT

The results obtained in simulation for the previously explained P&O algorithm will be shown in this section. First, the results corresponding to the PV panel model will be evaluated without connecting it to the DC-DC converter. Once the model for the PV panel is validated, the results obtained for the complete system will be analyzed in order to show the performance of the MPPT algorithm under different environmental conditions and resistive loads.

### 5.2.1 Model of the PV panel

This section shows the model and the results obtained from a commercial solar panel selected for the development of this project. The PV panel which will be utilized for the test of the MPPT is *Suntech STP300-24/Vd* [18]. As a result of the PV panel's model, the characteristic curves of the panel will be presented showing its behavior under variations in solar irradiance and temperature.

One of the most common methods for modeling a solar panel is using the equivalent circuit of a solar cell shown in figure 5.4. The model can be represented as a current source connected in antiparallel with a diode [14]. In addition, to model the non-linear behaviour of the solar panel I-V curve the equivalent series and parallel resistance ( $R_s$  and  $R_p$ ) are inserted [14].

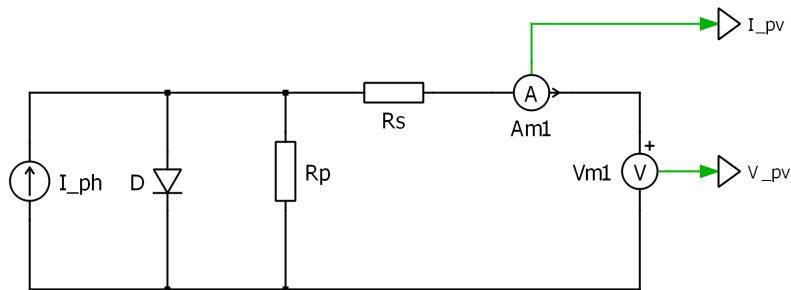


Figure 5.4: Equivalent circuit for modeling a PV cell.

The mathematical equation that describes the circuit is obtained applying Kirchoff's law to separate the current flowing through the different components of the circuit. This results in equation 5.3 where  $I_{pv}$  is the panel's current,  $I_{ph}$  is the photogenerated current, the second term is the current flow in the diode and the last term is the current flow in the parallel resistance [14].

$$I_{pv} = I_{ph} - I_o \cdot \left[ e^{\left( \frac{V_{pv} + R_s \cdot I_{pv}}{a \cdot V_t} \right)} - 1 \right] - \frac{V_{pv} + R_s \cdot I_{pv}}{R_p} \quad (5.3)$$

The second term corresponds to the Shockley equation where  $I_o$  is the saturation current of the diode,  $a$  is the diode's quality factor and  $V_t$  is the thermal voltage defined by

$$V_t = \frac{N_s \cdot K \cdot T}{q} \quad (5.4)$$

where  $N_s$  is the number of series connected cells (in this case 72),  $K$  is the Boltzmann constant ( $1.38 \cdot 10^{-23} \text{ J/K}$ ),  $T$  is the temperature in kelvins and  $q$  is the electrical charge ( $1.6 \cdot 10^{-19} \text{ C}$ ) [14].

However, as the focus of this project is not the modelling of the PV panel, the value of the PV panel's parameters such as  $R_s$ ,  $R_p$  and  $a$  required for the model will not be calculated. Instead, these values will be taken from the corresponding PV array block for the selected panel available in *Simulink*. All the values for the PV panel's electrical parameters corresponding to Standard Test Conditions (STC) are shown in table 5.1.

Electrical characteristics under Standard Test Conditions (STC)	
Maximum power ( $P_{max}$ )	300 [W]
Optimum Operating Voltage ( $V_{mpp}$ )	36.9 [V]
Optimum Operating Current ( $I_{mpp}$ )	8.14 [A]
Open Circuit Voltage ( $V_{oc}$ )	45 [V]
Short Circuit Current ( $I_{sc}$ )	8.67 [A]
Module Efficiency ( $\eta$ )	15.5 %
Operating Module Temperature	-40°C to +85°C
Series Resistance ( $R_s$ )	0.266 [Ω]
Parallel Resistance ( $R_p$ )	665.2 [Ω]
Diode quality factor ( $a$ )	1.1098

Table 5.1: Electrical characteristics PV module *Suntech STP300-24/Vd* [18].

Using the aforementioned model of the PV panel, it is possible to obtain the characteristic curves of the panel. Usually, PV panels are tested under STC to indicate the performance of the PV modules. The STC test is carried out at a solar cell's temperature of 25°C and at a solar irradiance of 1000 W/m<sup>2</sup> [2]. The higher the solar irradiance more power is generated from the PV panel. On the other hand, when the temperature of the PV cell increases the PV panel generates less power than at a lower temperature [2].

Figures 5.5 and 5.6 show the P-V and I-V curves of the solar panel with constant cell temperature ( $T = 25^\circ\text{C}$ ) and varying the level of irradiance. As expected, the lower the level of irradiance the maximum power that the panel is capable of generating decreases. It can be validated that under STC the values for  $V_{mpp}$  and  $I_{mpp}$  from table 5.1 correspond to the values obtained in simulation. Table 5.2 shows that a change in irradiance has as a consequence a high variation in  $I_{mpp}$  but  $V_{mpp}$  does not reflect a significant variation.

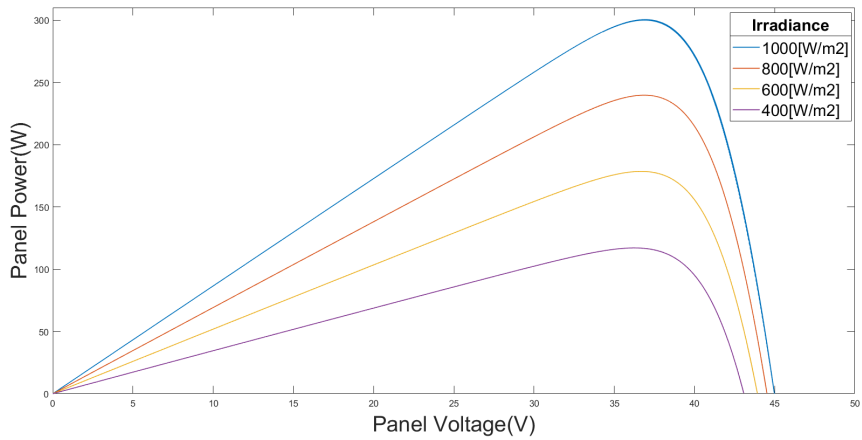


**Figure 5.5:** P-V curves for constant temperature ( $25^\circ\text{C}$ ) and change in irradiance.

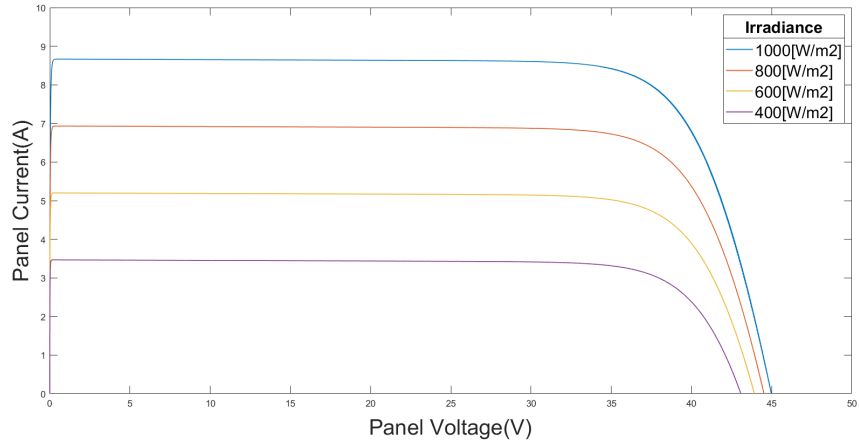


**Figure 5.6:** I-V curves for constant temperature ( $25^\circ\text{C}$ ) and change in irradiance.

<b>Constant temperature 25°C and varying irradiance</b>				
	1000W/m <sup>2</sup>	800W/m <sup>2</sup>	600W/m <sup>2</sup>	400W/m <sup>2</sup>
$V_{mpp}$ [V]	36.9	36.87	36.68	36.19
$I_{mpp}$ [A]	8.14	6.49	4.86	3.23
$P_{mpp}$ [W]	300.4	239.5	178.5	117

**Table 5.2:** Results of the optimum PV panel parameters for varying irradiance.

On the other hand, figures 5.7 and 5.8 show the characteristic curves with constant irradiance ( $1000W/m^2$ ) and under temperature variation.

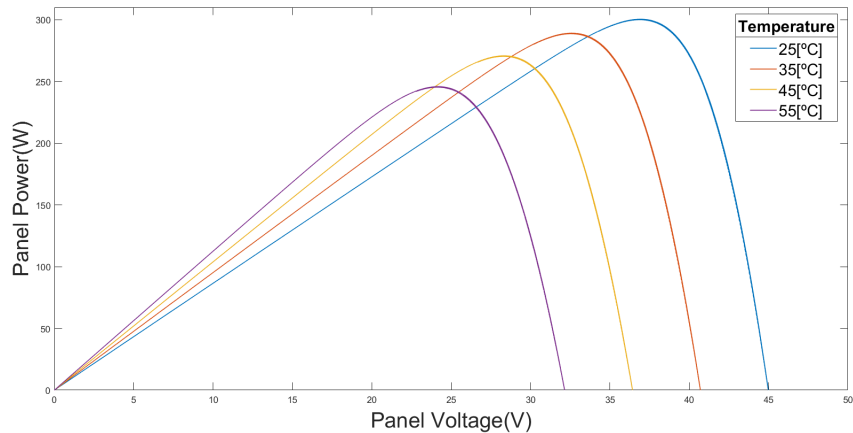


**Figure 5.7:** P-V curves for constant irradiance ( $1000W/m^2$ ) and change in temperature.

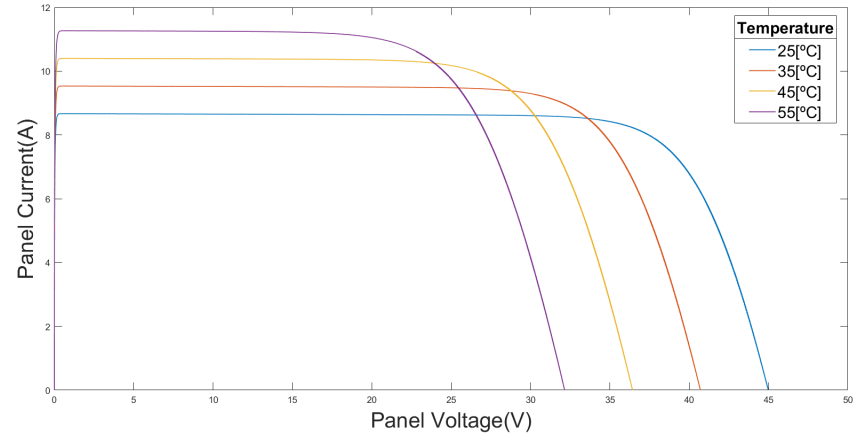


**Figure 5.8:** I-V curves for constant irradiance ( $1000W/m^2$ ) and change in temperature.

It is observed from table 5.3 that an increase in the temperature means that the maximum power that the panel is able to generate decreases. In this case, a change in temperature has as a consequence a high variation of  $V_{mpp}$ . However, the variation is not that significant in  $I_{mpp}$ .

Constant irradiance $1000W/m^2$ and varying temperature				
	T=25°C	T=35°C	T=45°C	T=55°C
$V_{mpp}$ [V]	36.9	32.59	28.34	24.23
$I_{mpp}$ [A]	8.14	8.85	9.59	10.12
$P_{mpp}$ [W]	300.4	289.1	270.7	245.8

Table 5.3: Results of the optimum PV panel parameters for varying temperature.

### 5.2.2 Simulation results

In this section, the results obtained in simulation for the entire system will be presented. The system includes the solar panel, the non-inverting buck-boost converter and the MPPT controller unit as shown in figure 5.1. The simulated results will be analyzed to determine the performance of the MPPT and will be divided in two parts:

- Results obtained under STC. The STC test is carried out at a solar cell's temperature of 25°C and at a solar irradiance of  $1000 W/m^2$  [2].
- Results obtained under a sudden change in the solar irradiance and temperature.

It was decided to use a resistive load to validate the results obtained in the simulation with the experimental results. All the simulations will be carried out for two different resistive loads:  $R_L = 3\Omega$  and  $R_L = 27\Omega$ . This is done in order to validate the performance of the MPPT controller in both modes of operation.

#### Standard Test Conditions (STC)

Figure 5.9 shows how the P&O algorithm searches for the MPP. The first graph shows a superposition of the PV panel's voltage and current where it is observed that the panel reaches the open-circuit voltage ( $V_{oc} = 45V$ ) and at that moment the MPPT starts searching for the MPP by decreasing the PV voltage. The second graph shows the power generated by the panel which approaches the value of the optimal power under this conditions ( $P_{mpp} = 300W$ ). The P&O algorithm converges to the MPP reaching the steady state in 2 seconds. The MPPT allows to reach the optimal power generated by the panel under this conditions with an efficiency of  $\eta_{MPPT} = 99.96\%$ .

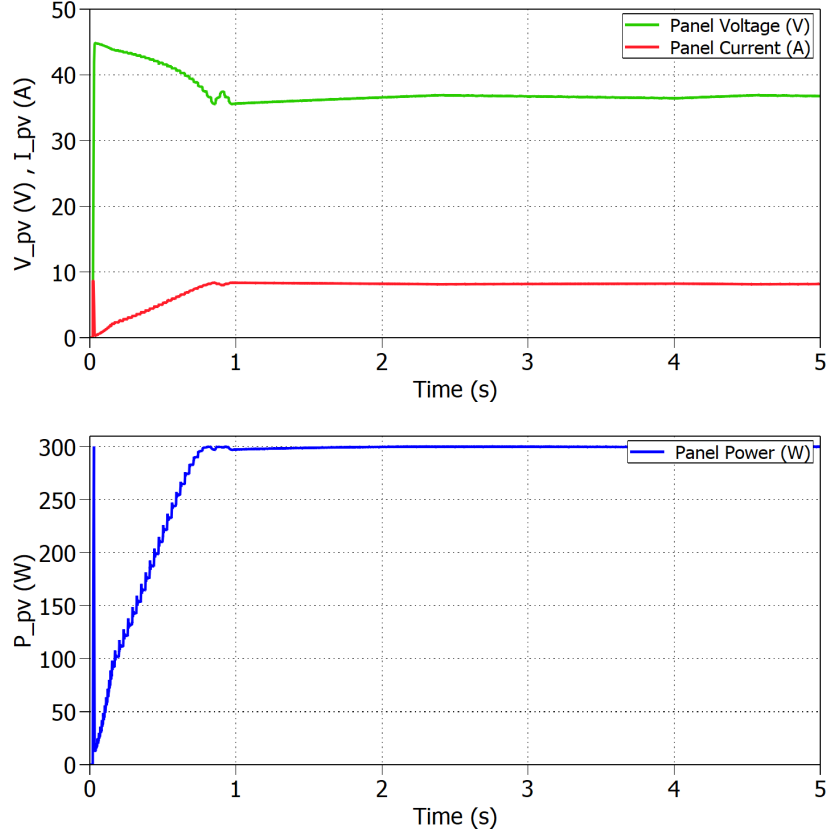


Figure 5.9: Voltage, current and power extracted from the PV panel ( $R_L = 3\Omega$ ).

The simulation is run under STC and using a resistive load of  $3\Omega$ . From the first graph of figure 5.10 it is observed that the converter is working in buck mode during all the MPPT process. This is because the output voltage does not exceed the input voltage with this resistive load as shown in the second graph. The value of the duty cycle, obtained in simulation under these load and environment conditions, is  $D_{buck} = 0.8155$ . Using the transfer function of the converter in buck mode, this value can be validated by calculating the theoretical duty cycle taking as voltage input  $V_{mpp} = 36.9V$ :

$$\frac{V_o}{V_i} = D \rightarrow D = \frac{30V}{36.9V} = 0.8130 \quad (5.5)$$

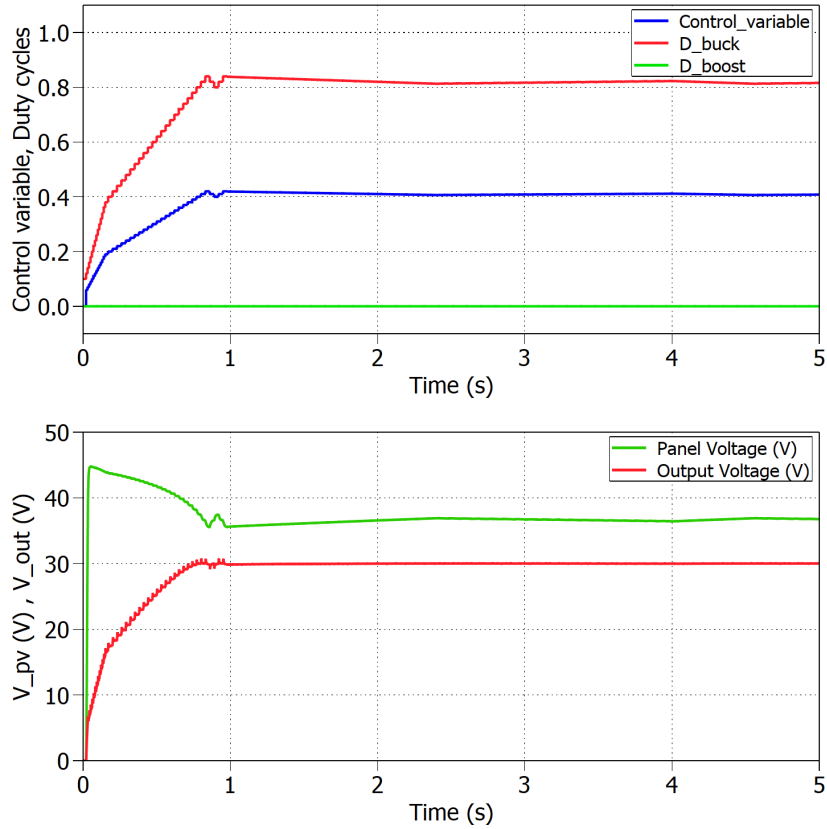
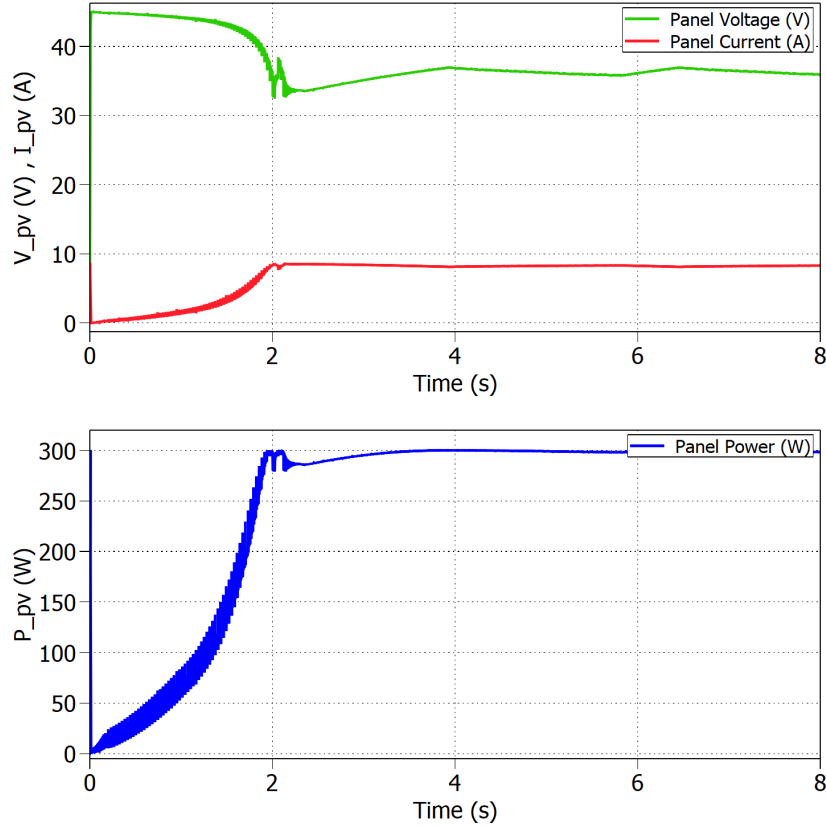


Figure 5.10: Converter's mode of operation as a function of the control variable ( $R_L = 3\Omega$ ).

The same simulation was implemented but in this case using a value of the resistive load of  $27\Omega$ . From figure 5.11 it is observed that the MPPT needs more time than before to converge to the MPP. The P&O algorithm needs 4 seconds to reach the MPP which means double of the time than with  $R_L = 3\Omega$ . This occurs because the output voltage starts increasing from 0 to its final value. This means that the system will start working in buck mode and once the output voltage reaches the value of the input voltage it will switch to boost mode. Despite the higher converging time to the MPP, the P&O algorithm performance has not experienced a significant difference. The MPPT is able to operate with an efficiency of  $\eta_{MPPT} = 99.82\%$ .



**Figure 5.11:** Voltage, current and power extracted from the PV panel ( $R_L = 27\Omega$ ).

Figure 5.12 shows how the converter starts operating in buck mode until the output voltage equals the input voltage. At this point is the limit between the two modes of operation and the converter starts working in boost mode. The value of the duty cycle under these load and environment conditions is  $D_{boost} = 0.5971$ . Using the transfer function of the converter in buck mode, this value can be validated by calculating the theoretical duty cycle taking as voltage input  $V_{mpp} = 36.9V$ :

$$\frac{V_o}{V_i} = \frac{1}{1 - D} \rightarrow D = 1 - \frac{V_i}{V_o} = 1 - \frac{36.9}{90} = 0.5900 \quad (5.6)$$

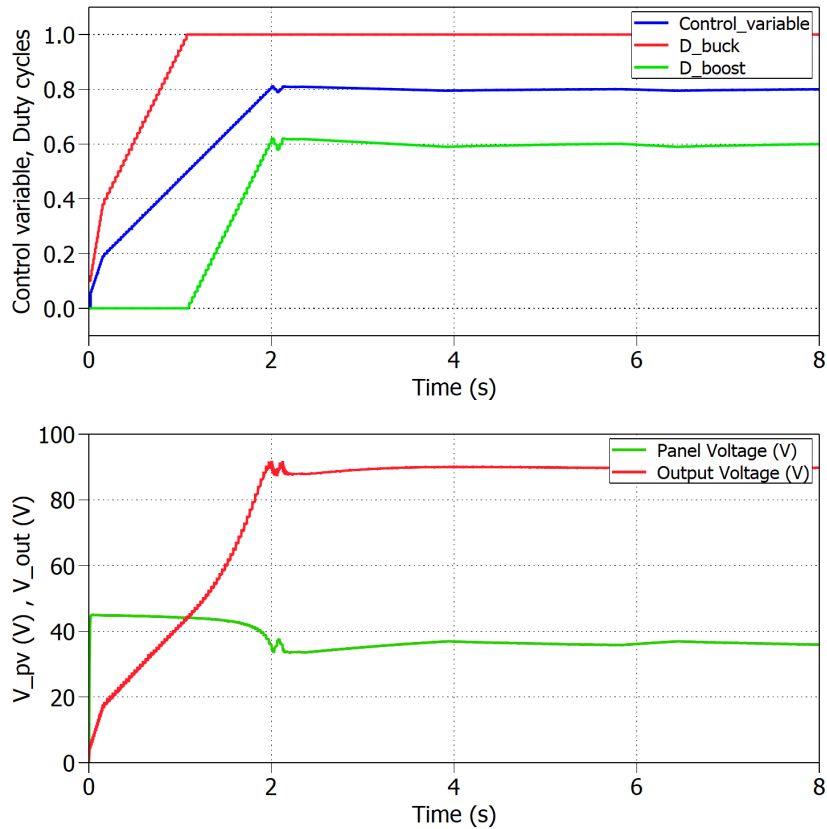
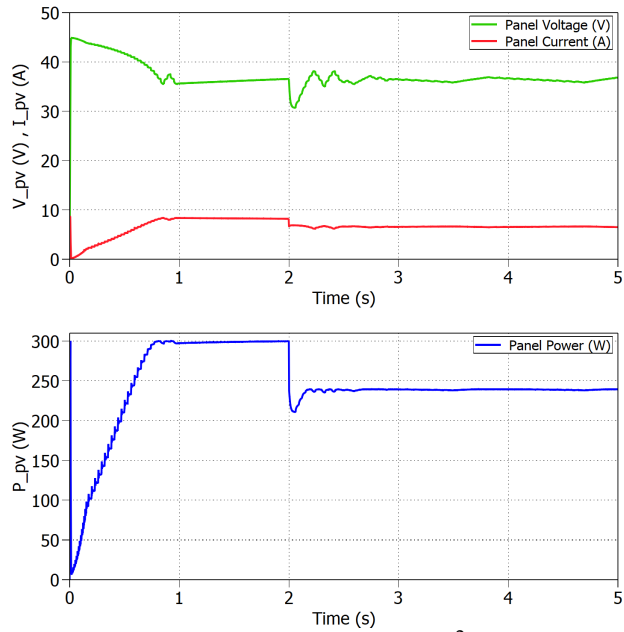
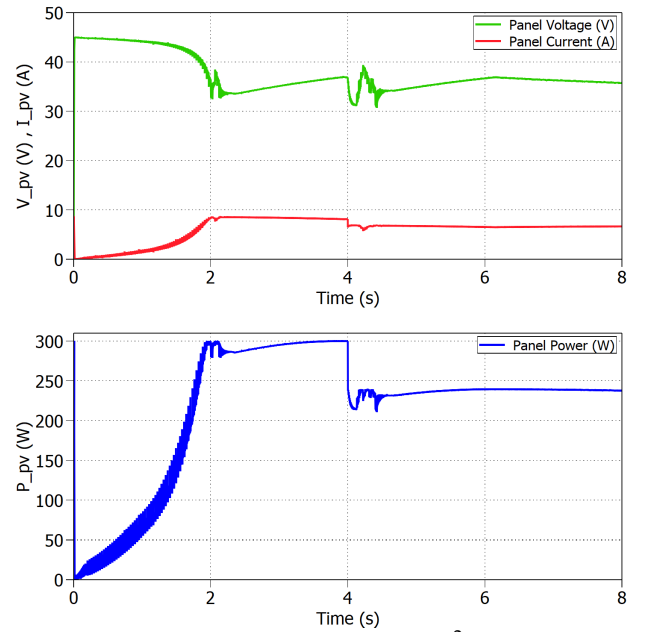
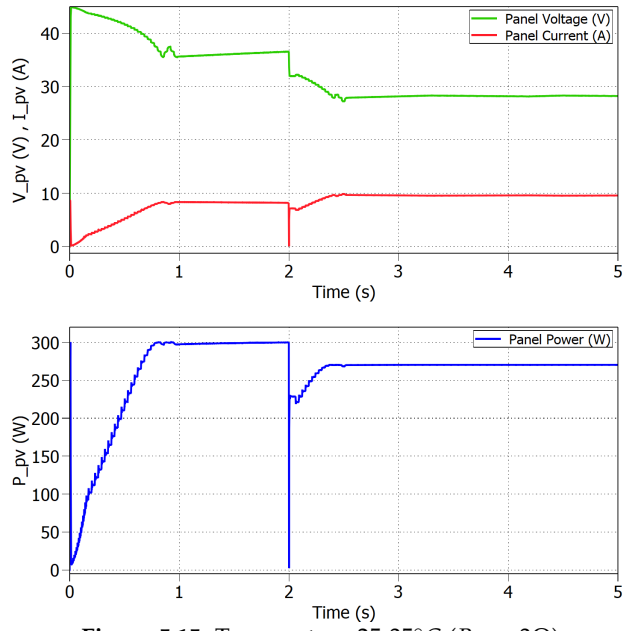
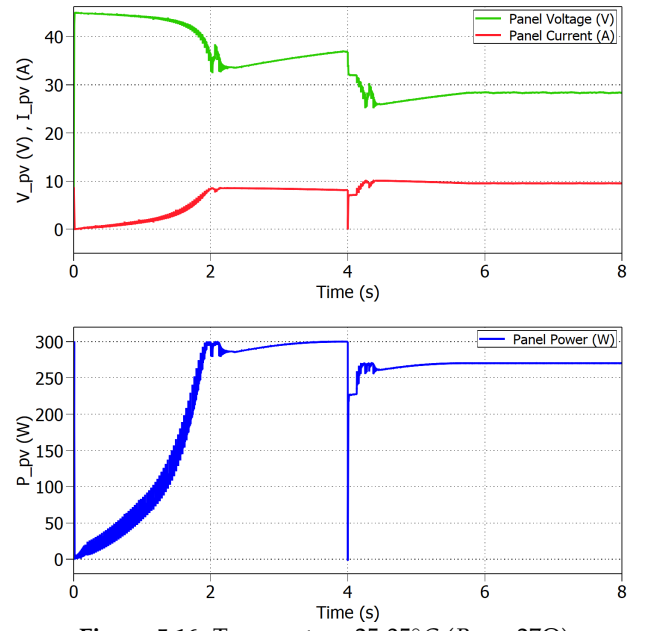


Figure 5.12: Converter's mode of operation as a function of the control variable ( $R_L = 27\Omega$ ).

### Change in irradiance and temperature

This section shows the performance of the MPPT when the PV panel is exposed to a sudden change in irradiance and in temperature. First, figures 5.13 and 5.14 show the results obtained for a change in irradiance for the case of buck and boost mode, respectively. The irradiance change is from  $1000 \text{ W/m}^2$  to  $800 \text{ W/m}^2$  while the cell temperature is kept constant at  $25^\circ\text{C}$ . Figures 5.15 and 5.16 show the results for a sudden increase of the solar cell's temperature for both modes of operation. The temperature changes from  $25^\circ\text{C}$  to  $35^\circ\text{C}$  by keeping constant the irradiance to a value of  $1000 \text{ W/m}^2$ . In all the cases the P&O algorithm can track the MPP by maintaining an efficiency higher than 99%. This way it is validated that the MPPT algorithm works efficiently under sudden changes of irradiance and temperature. However, this situations are not realistic because in real environmental conditions the sunlight and the temperature will not experience such a sudden change.

Figure 5.13: Irradiance  $1000-800\text{W}/\text{m}^2$  ( $R_L = 3\Omega$ ).Figure 5.14: Irradiance  $1000-800\text{W}/\text{m}^2$  ( $R_L = 27\Omega$ ).Figure 5.15: Temperature  $25-35^\circ\text{C}$  ( $R_L = 3\Omega$ ).Figure 5.16: Temperature  $25-35^\circ\text{C}$  ( $R_L = 27\Omega$ ).



# 6

## Test and validation of results

When the design stage is completed, it must be validated. The system design consisted of hardware and control design. The validation checks whether the system is compliant with the initial goals. The validation is performed in two steps: first the design is validated through software simulation. This step was explained in previous chapters. The second step consists on the validation over the physical implementation and will be addressed in this chapter.

The hardware design testing is performed following an incremental fashion. The components are individually soldered to the PCB and tested. The tests are short and with clear boundaries. This features ease the errors' finding and troubleshooting. This procedure validates the proper behaviour in the single component but also lets analyse the effect of additional components. The assembly and test procedure will be defined prior to the PCB assembly. The tests and its expected results are clear before starting. When the PCB is assembled and all the integration tests are passed, the complete converter is tested. This system test is performed by running the converter with a fixed duty cycle. This test allows the validation of the converter as a whole, including voltage and current ripples, thermal test, gain and losses.

The control design testing must demonstrate that the control signals are properly calculated in order to achieve maximum power generation. These signals are received by the previously tested hardware implementation. The testing consists on black box testing where only a few internal parameters are monitored through the controller's console. The system's stability and dynamic behaviour will analysed.

## 6.1 PCB building

The building of the PCB in iteration one of the development has been done according to the test described in the following section. It has been divided into smaller tests, to validate that every part of the system works properly. The first part is the test of the control part, so the optocouplers, drivers and sensors. The last part is then the test of the power stage of the converter. It has been chosen only to solder the buck leg of the converter to validate the design, and discover faults which must be dealt with in iteration two. Before starting the test all vias, capacitors and test-points are soldered to assure connectivity.

### 6.1.1 Power supplies

The purpose of the first test was to validate the different power supplies in the converter. For this test it's necessary to solder the in-TRACO and the 5V voltage regulator. The three LED's and the resistors should also be soldered. Apply 5V at connector J4 and 12V at connector J2. The test is conducted by following table 6.1

The tables will be resized to fit the page.

Test of power supplies			
ID	Test	Test-points	Pass/Fail
1.1	All LED's must be lit	DS1-2-4	Pass
1.2	Measure 5V at low-voltage	5V-LV & GND-LV	Pass
1.3	Measure 12V at high voltage, low-side	12V & GND-in	Pass
1.4	Measure 12V at output of in-TRACO	12V-in & L-in	Pass
1.5	Measure 5V at the output of the voltage regulator	5V-HV & GND-sen	Pass

Table 6.1: Test of power supplies.

### 6.1.2 Optocouplers

The second part of the test is to validate the optocouplers. This includes that the output of the optocoupler should follow the input. For this test it's necessary to solder opto1-2, and an extra test-point at the output of the two optocouplers. Because of a wrongly chosen optocoupler with a supply voltage at 5V, a voltage divider must be added. This will be placed between the supply pins of the IC, and will divide 12V into 5V. Start the test by applying 5V at connector J4, 12V at connector J2 and a 5V – 50kHz square waveform with 50% duty-cycle at PWM1-2.

<b>Test of optocouplers</b>			
<b>ID</b>	<b>Test</b>	<b>Test-points</b>	<b>Pass/Fail</b>
2.1	Measure 5V at the supply of opto1-2	IC pin 6(+) & 4(-)	Pass
2.2	Measure 5V – 50kHz at the input of optocoupler 1	TST1 & GND-LV	Pass
2.3	Measure 5V – 50kHz at the output of optocoupler 1	Opto1-out & L-in	Pass
2.4	Measure 5V – 50kHz at the input of optocoupler 2	TST2 & GND-LV	Pass
2.5	Measure 5V – 50kHz at the output of optocoupler 2	Opto2-out & GND-in	Pass

**Table 6.2:** Test of the optocouplers.

### 6.1.3 Drivers

The next part of the test consist of the drivers. For this it's necessary to solder drv1-2, M1-2 and the resistors R5-R10. The input threshold of the drivers is defined as  $V_{DD} - 3.1V$ . Because of the 5V optocouplers, the supply voltage of the drivers must be lowered to 5V, for the switching to work. A consequence of this is that the voltage divider that supplies the optocoupler should be removed. Start the test by applying 5V at connector J2 & J4 and a 5V – 50kHz square waveform with 50% duty-cycle at PWM1-2. The test is conducted by following table 6.3.

<b>Test of drivers</b>			
<b>ID</b>	<b>Test</b>	<b>Test-points</b>	<b>Pass/Fail</b>
3.1	Measure 5V at the supply of the drivers	IC pin 6-7(+) & 2-3(-)	Pass
3.2	Measure 5V – 50kHz at the output of driver 1	PWM1 & L-in	Pass
3.3	Measure 5V – 50kHz at the output of driver 2	PWM2 & GND-in	Pass

**Table 6.3:** Test of the drivers.

### 6.1.4 Sensors

The last part of the control system test consist of the sensor circuits. For this test it's necessary to solder the input voltage sensor U12, the current sensor and the operational amplifier. Furthermore the resistors  $R_{17} - R_{22} + R_{25} + R_{32} + R_{33}$  and capacitors  $C_{17} + C_{22}$  should be soldered. Before testing a jumper should be placed between J5-2 and J5-3, to select the bandwidth of the current sensor to 80kHz. The inductor, M1 and M3 should also be shorted to achieve a current flow through the

current sensor.

Attach a load resistor at  $100\Omega$ . With an input voltage at  $10V$ , this should correspond to a output current at  $100mA$ . Because of the differential offset in the current sensor, this should be equal to  $2.6V$ . After test 4.3, raise the input voltage to  $20V$  for validation of linearity in the sensors.

<b>Test of sensors</b>			
<b>ID</b>	<b>Test</b>	<b>Test-points</b>	<b>Pass/Fail</b>
4.1	Measure $10V$ at the input of the converter	Vin & GND-in	Pass
4.2	Measure $1V$ at the output of the voltage sensor	Vi-sen & GND-sen	Pass
4.3	Measure $2.6V$ at the output of the current sensor	IL-sen-Raw & GND-sen	Pass
4.4	Measure $20V$ at the input of the converter	Vin & GND-in	Pass
4.5	Measure $2V$ at the output of the voltage sensor	Vi-sen & GND-sen	Pass
4.6	Measure $2.7V$ at the output of the current sensor	IL-sen-Raw & GND-sen	Pass

**Table 6.4:** Test of the sensors.

## 6.2 MPPT

### 6.2.1 RT-box

### 6.2.2 PV simulator

### 6.2.3 Load

### 6.2.4 Experimental results

# 7

## Discussion

we will write here a little part about the iteration 1, which problem we have and how we fix it.



8

## Conclusion

to-do



# Bibliography

- [1] J. Rutovitz J. L. Sawing and F. Sverrisson. "*Renewables 2018 Global Status Report*". ISBN 978-3-9818911-3-3. Paris, France: REN21, 2018. 325 pp.
- [2] M. Boxwell. "*Solar Electricity Handbook*". 11th Edition. Greenstream Publishing Limited. 212 pp. URL: <http://www.sabz-energy.com/solar%20electricity%20handbook%202017.pdf>.
- [3] N. Henze B. P. Koirala B. Sahan. "*Study on MPP mismatch losses in photovoltaic applications*". Germany: Institute of Solar Energy Technology, Sept. 25, 2014. 7 pp.
- [4] A. Baker. "*A history of solar cells: how technology has evolved*". Solar Power Authority. Sept. 2018. URL: <https://www.solarpowerauthority.com/a-history-of-solar-cells/>.
- [5] "*Solar cell I-V characteristic*". Sept. 2018. URL: <http://www.alternative-energy-tutorials.com/energy-articles/solar-cell-i-v-characteristic.html>.
- [6] M. Rosu-Hamzescu and S. Oprea. "*Practical Guide to Implementing Solar Panel MPPT Algorithms*". Microchip Technology Inc., 2013. 16 pp.
- [7] D. Bromberg. "*Know how inverter MPPT functionality affects performance*". Aurora Solar. Mar. 7, 2018. URL: <https://www.solarpowerworldonline.com/2018/03/install-tip-inverter-mppt-functionality-affects-performance/>.
- [8] D. Clement C. Olalla and M. Rodriguez. "*Architectures and control of submodule integrated DC-DC converters for photovoltaic applications*". Vol.28, No.6. IEEE Transactions on power electronics, June 6, 2013. 18 pp.

- [9] H. Tran M. Q. Duong and C. A. Hossain. "*Influence of elemental parameter in the boost and the buck converter*". IEEE Region 10 Humanitarian Technology Conference. Dhaka, Bangladesh: The University of Danang. 4 pp.
- [10] ROHM Semiconductor. "*Efficiency of buck converter*". ROHM Co., Ltd., Dec. 2016. 16 pp.
- [11] N. H. Baharudin et al. "*Topologies of DC-DC converter in solar PV applications*". Vol.8, No.2. Universiti Malaysia Perlis (UniMAP): Indonesian Journal of Electrical Engineering and Computer Science. 7 pp.
- [12] T. Hegarty V. Choudhary and D. Pace. "*Under the hood of a non-inverting buck-boost converter*". Dallas, Texas: Texas Instruments, Sept. 1, 2016. 25 pp.
- [13] STMicroelectronics. "*Buck-boost converter using the STM32F334 Discovery kit, AN4449*". 34 pp.
- [14] M. Gomes de Brito et al. "*Evaluation of the main MPPT techniques for photovoltaic applications*". Vol.60, No.3. IEEE Transaccions on industrial electronics, Mar. 3, 2013. 12 pp.
- [15] Y. Verma P. Gaur and P. Singh. "*Maximum power point tracking algorithms for photovoltaic applications: a comparative study*". Chandigarh, India: Panjab University, Dec. 21, 2015. 5 pp.
- [16] S. Kim et al. "*Photovoltaic Maximum Power Point Tracking without Current Sensor for Module Integrated Converter*". Beijing, China: International Conference on Electrical Machines and Systems, Aug. 20, 2011.
- [17] A. Nigam and K. Gupta. "*Performance and simulation between conventional and improved perturb and observe MPPT algorithm for solar PV cell using MATLAB/Simulink*". Allahabad, India: International Conference on Control, Computing, Communication and Materials, Oct. 21, 2016.
- [18] Suntech Power. *PV-module SuperPoly. STP300-24/Vd Datasheet*. 2012. URL: [http://www.selasenergy.gr/technical%20data/solar-panels/suntech/20120522%20Q3Superpoly\\_Vd\\_305\(H4\\_305\\_300\\_295\)\\_EN\\_WEB.pdf](http://www.selasenergy.gr/technical%20data/solar-panels/suntech/20120522%20Q3Superpoly_Vd_305(H4_305_300_295)_EN_WEB.pdf).
- [19] Power-One. *Specification of power-one microsystems solar grid tie string inverter 1 - 5 kW*. 2018. URL: <https://www.enfsolar.com/Product/pdf/Inverter/56f9df850ce92.pdf>.
- [20] R. W. Erickson and D. Maksimovic. "*Fundamentals of Power Electronics*". 2nd Edition. Kluwer Academic Publishers, 2004. 883 pp. URL: [https://eleccompengineering.files.wordpress.com/2015/01/fundamentals-of-power-electronics\\_2nd\\_erickson\\_full.pdf](https://eleccompengineering.files.wordpress.com/2015/01/fundamentals-of-power-electronics_2nd_erickson_full.pdf).
- [21] Panasonic. *Type 381LQ 105 °C compact, high ripple, snap-in aluminum. 381LQ821M250K032 Datasheet*. 2018. URL: <https://docs-emea.rs-online.com/webdocs/13e5/0900766b813e53d3.pdf>.

- [22] Panasonic. *Aluminum electrolytic capacitors/FC. EEUFC2A471 Datasheet*. June 7, 2015. URL: <https://docs-emea.rs-online.com/webdocs/1489/0900766b8148953c.pdf>.
- [23] D. Costinett. "Lecture 7: MOSFET, IGBT, and Switching Loss". Ed. by University of Tennessee Knoxville. Department of Electrical Engineering and Computer Science, University of Tennessee Knoxville. 2013. URL: [http://web.eecs.utk.edu/~dcostine/ECE481/fall2013/lectures/L7\\_slides.pdf](http://web.eecs.utk.edu/~dcostine/ECE481/fall2013/lectures/L7_slides.pdf).
- [24] C. Blake and C. Bull. "IGBT or MOSFET: Choose Wisely". Ed. by International Rectifier. Nov. 13, 2018. URL: [https://www.infineon.com/dgdl/Infineon-IGBT\\_or\\_MOSFET\\_ChOOSE\\_Wisely-ART-v01\\_00-EN.pdf?fileId=5546d462533600a40153574048b73edc](https://www.infineon.com/dgdl/Infineon-IGBT_or_MOSFET_ChOOSE_Wisely-ART-v01_00-EN.pdf?fileId=5546d462533600a40153574048b73edc).
- [25] Infineon Technologies AG. *OptiMOS 3 Power-Transistor. IPB200N15N3GATMA1 Datasheet*. URL: <https://docs-emea.rs-online.com/webdocs/1090/0900766b810908e8.pdf>.
- [26] Thermo Electric Devices. *Extruded heat sink / Fan assembly. TDEX6015/TH12G Datasheet*. May 2, 2014. URL: <https://docs-emea.rs-online.com/webdocs/0b05/0900766b80b0587d.pdf>.
- [27] AVAGO Technologies. *0.4 Amp Output Current IGBT Gate Driver Optocouplers. ACPL-P302/W302 Datasheet*. Dec. 10, 2010. URL: <https://docs-emea.rs-online.com/webdocs/0f8b/0900766b80f8ba5c.pdf>.
- [28] ON Semiconductor. *Single channel 10A high speed low-side MOSFET driver*. Nov. 1, 2015.
- [29] TT Electronics. *Pulse withstanding resistors. Application note Datasheet*. Nov. 1, 2015. URL: [http://www.ttelectronics.com/themes/ttelectronics/datasheets/resistors/literature/pwc\\_appnotes.pdf](http://www.ttelectronics.com/themes/ttelectronics/datasheets/resistors/literature/pwc_appnotes.pdf).
- [30] Infineon. *EiceDRIVER™: Gate resistor for power devices. Application Note AN2015-06 Datasheet*. Dec. 17, 2015. URL: [https://www.infineon.com/dgdl/Infineon-EiceDRIVER - Gate + resistor + for + power + devices - AN - v01\\_00 - EN.pdf?fileId=5546d462518ffd8501523ee694b74f18](https://www.infineon.com/dgdl/Infineon-EiceDRIVER - Gate + resistor + for + power + devices - AN - v01_00 - EN.pdf?fileId=5546d462518ffd8501523ee694b74f18).
- [31] Avago Technologies. *Precision Optically Isolated Voltage Sensor. ACPL-C87B, ACPL-C87A, ACPL-C870 Datasheet*. Mar. 4, 2013. URL: <https://docs-emea.rs-online.com/webdocs/116c/0900766b8116c0f3.pdf>.
- [32] Texas Instruments. *LMC6484 CMOS quad rail-to-rail input and output operational amplifier*. Sept. 2015. URL: <http://www.ti.com/lit/ds/symlink/lmc6484.pdf?fbclid=IwAR2-z4SAec11ZMHQGk9z1CUVKjUphWbEPVIUkoxwhvqehAp6lwYe6sYFbk>.

- [33] Allegro MicroSystems LLC. *High Accuracy, Galvanically Isolated Current Sensor IC With Small Footprint SOIC8 Package. ACS723 Datasheet*. Oct. 6, 2014. URL: <https://docs-emea.rs-online.com/webdocs/13b5/0900766b813b538e.pdf>.
- [34] Traco Power. *DC/DC Converters. TMA series 1 Watt Datasheet*. Feb. 11, 2014. URL: <https://docs-emea.rs-online.com/webdocs/153a/0900766b8153aa01.pdf>.
- [35] ST Microelectronics. *Low drop fixed and adjustable positive voltage regulators. LD1117xx Datasheet*. July 2009. URL: <https://docs-emea.rs-online.com/webdocs/0dbd/0900766b80dbda35.pdf>.
- [36] S. Ahmed A. K. Abdelsalam A. M. Massoud and P. N. Enjeti. "High-performance adaptive perturb and observe MPPT technique for photovoltaic-based microgrids". Vol.26, No.4. Doha, Qatar: IEEE transactions on power electronics. 12 pp.
- [37] M. Kamil. "Switch Mode Power Supply (SMPS) Topologies (Part I)". Microchip Technology Inc., 2017. 48 pp.
- [38] B. Hauke. "Basic calculation of a buck converter's power stage". Texas Instruments. 8 pp.
- [39] B. Hauke. "Basic calculation of a boost converter's power stage". Texas Instruments. 9 pp.

A

## PCB schematics and Layout

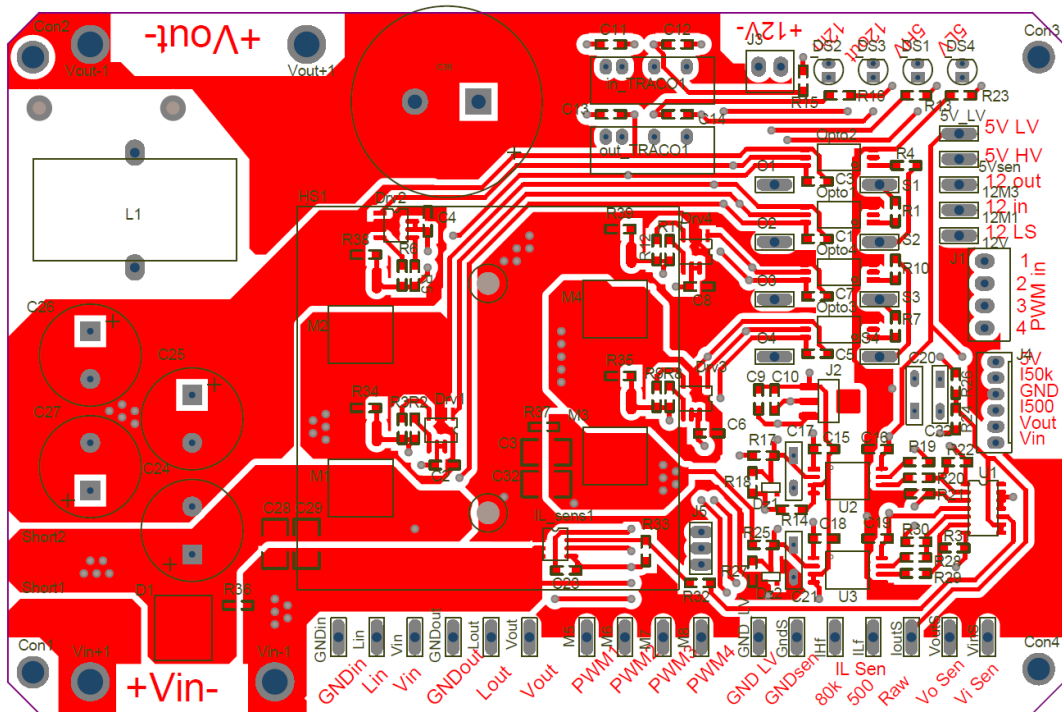


Figure A.1: PCB top layer.

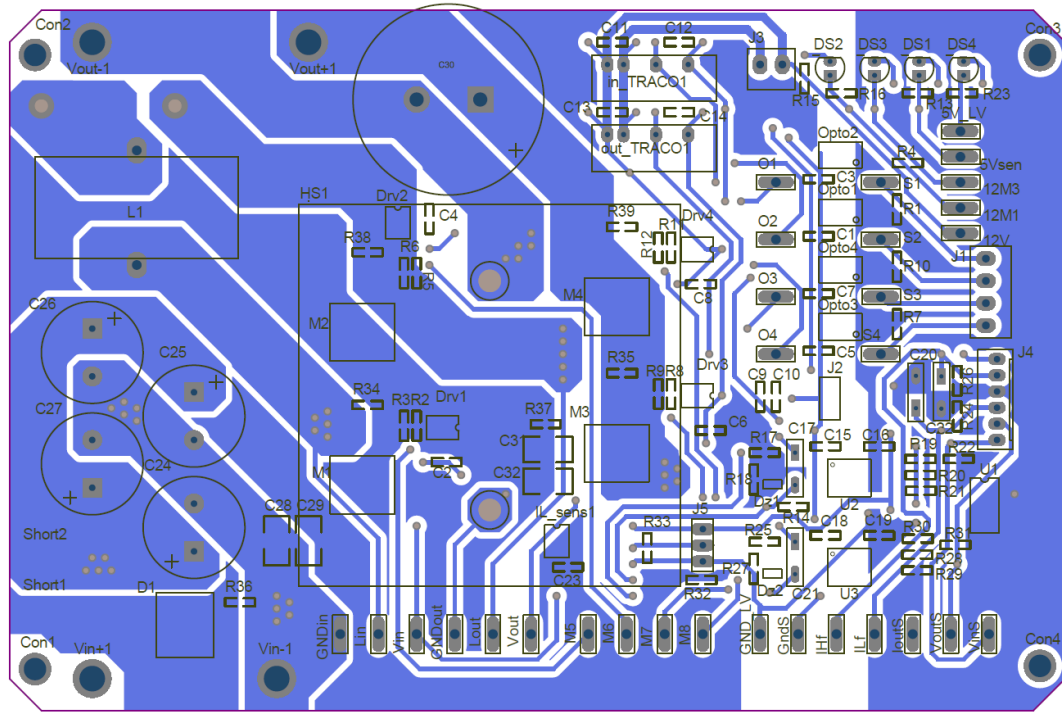
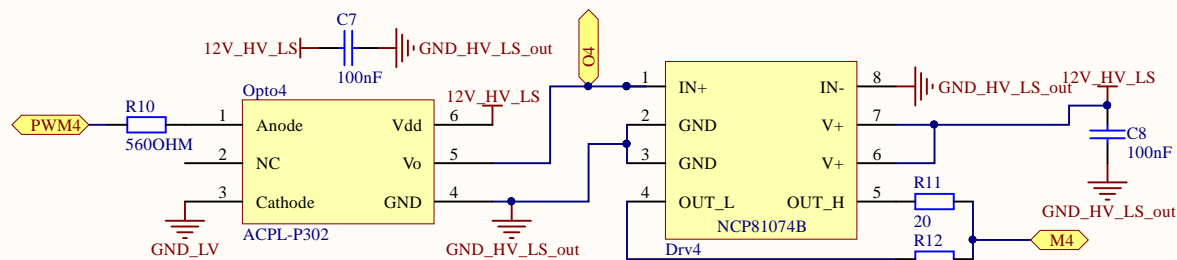
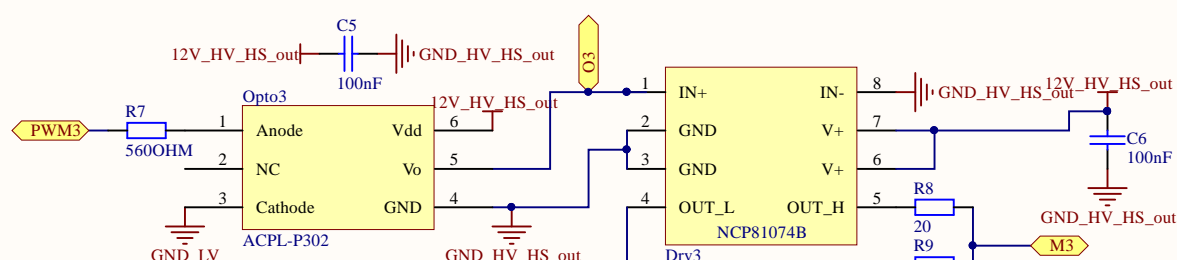
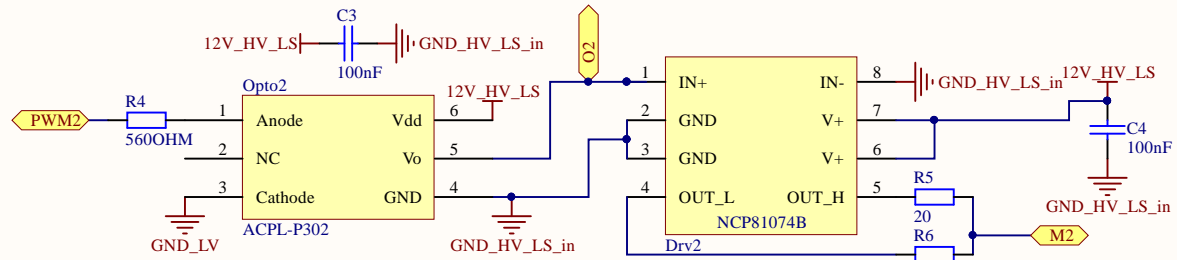
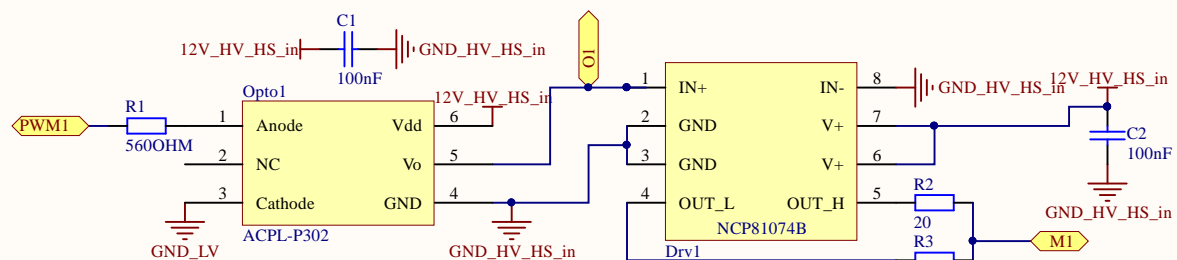
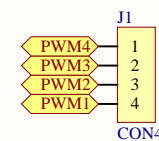
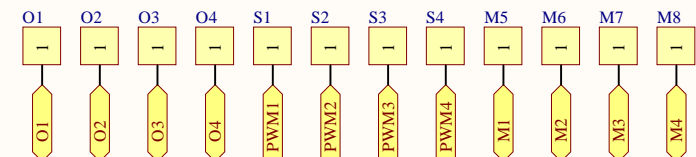
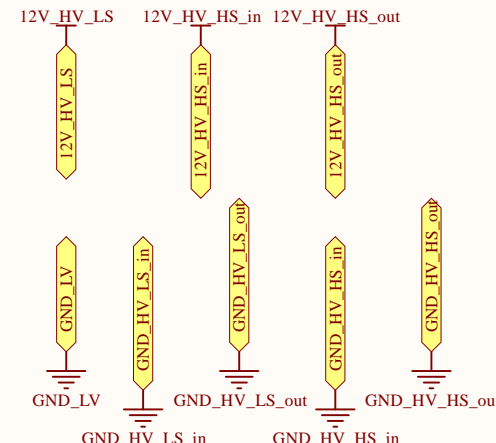


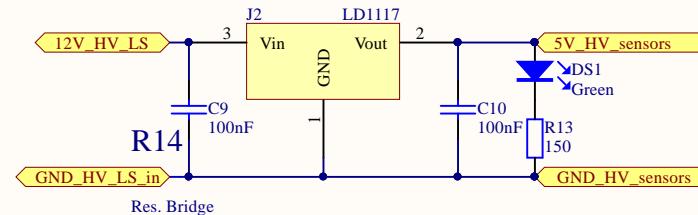
Figure A.2: PCB bottom layer.

**DRIVER CIRCUIT****From RT Box****Test Points****Global Connections**

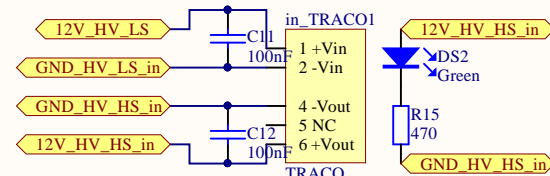
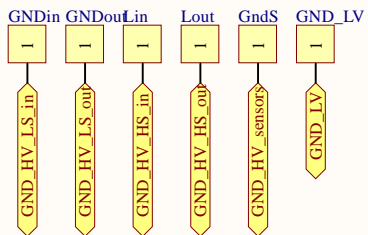
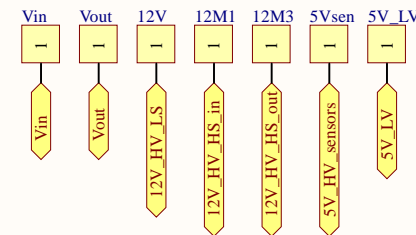
Title  
**Optocouplers and driver circuitry**

Size	Number	Revision
A4		
Date: 05/12/2018	Sheet 2 of 4	
File: C:\Users\...\Drivers_V2.SchDoc		Drawn By: nsn-760

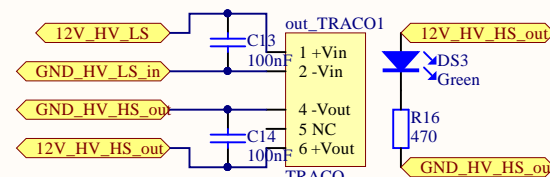
A

**Input Voltage****Sensors 5V signal**

B

**Traco Power****Test Points****Grounds****Voltages**

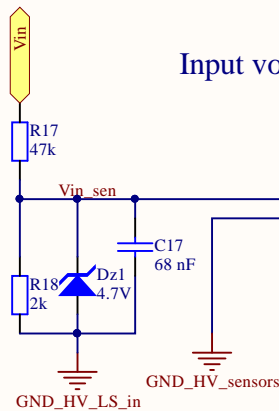
C



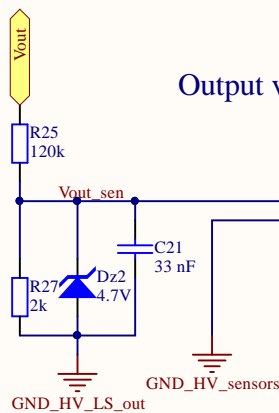
D

Title  
**Power supplies**  
Size  
A4  
Number  
Revision

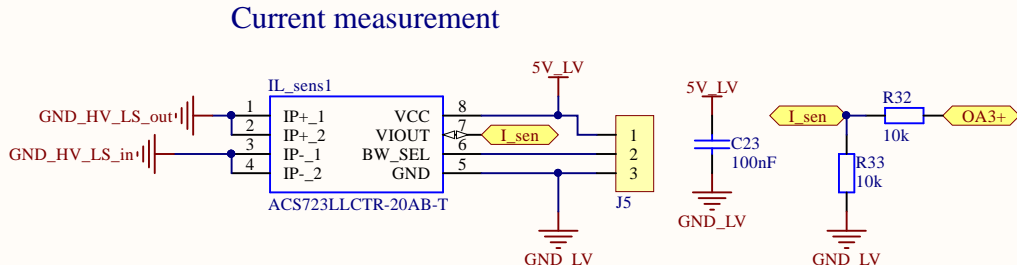
Date:	05/12/2018	Sheet 3 of 4
File:	C:\Users\.\Power_supplies_V2.SchDoc	Drawn By: nsn-760



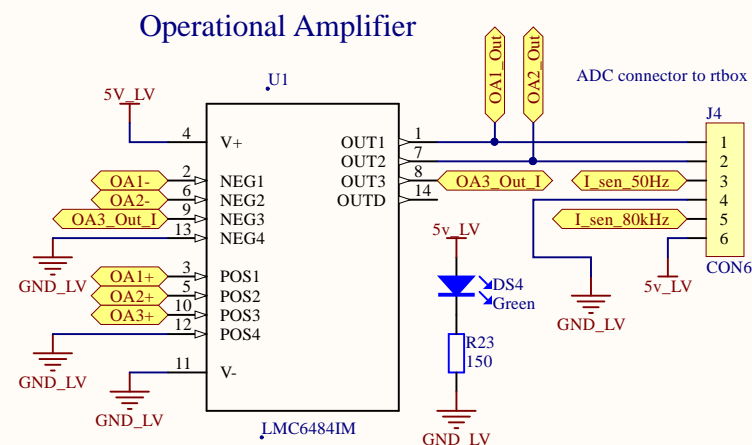
Input voltage measurement



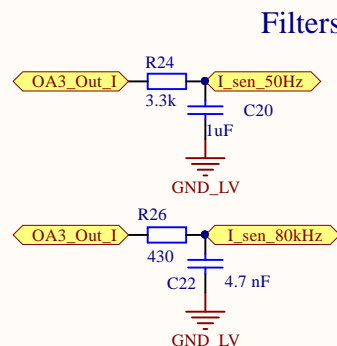
Output voltage measurement



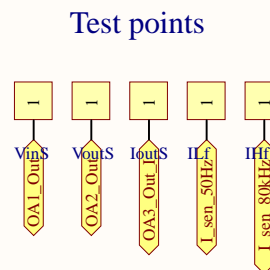
Current measurement



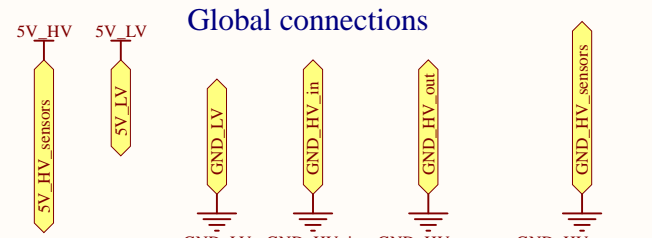
Operational Amplifier



Filters



Test points



Global connections

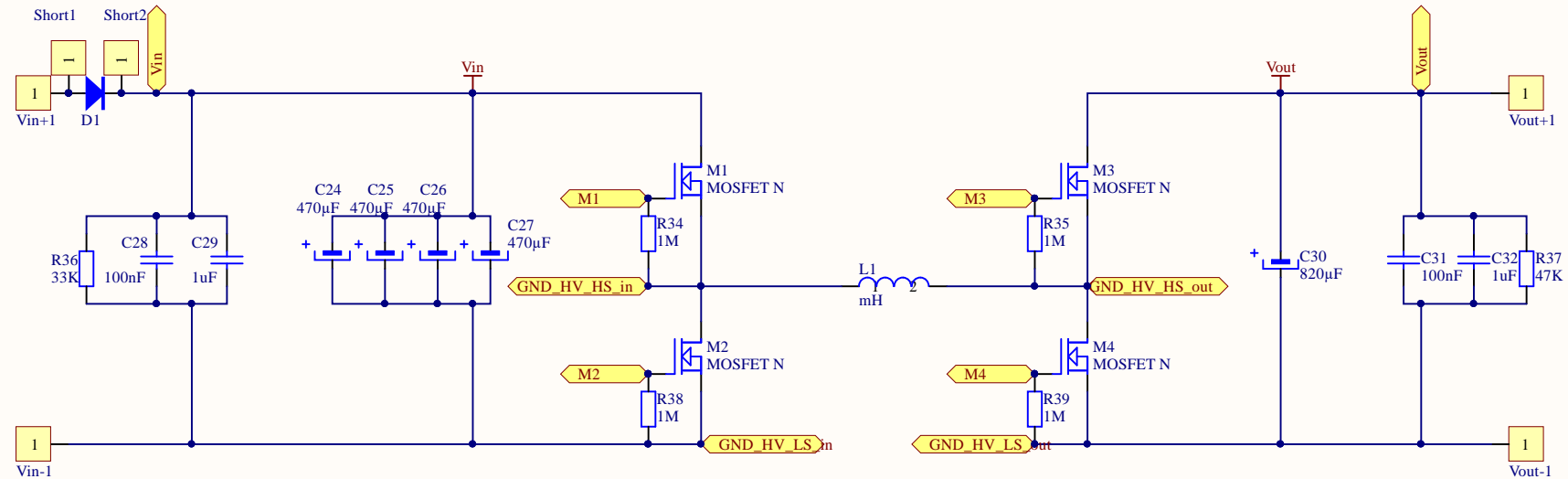
Title  
Sensors and signal processing

Size	Number	Revision
A4		
Date:	05/12/2018	Sheet 4 of 4
File:	C:\Users...\Signal_processing_V2.SchD	Drawn By: nsn-760

A

A

## Main Topology



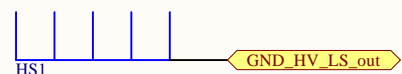
B

B

C

C

### Heatsink



### Support holes



Title Power switches and passive components		
Size A4	Number	Revision
Date: 05/12/2018	Sheet 1 of 4	
File: C:\Users\...\Switches_V2.SchDoc	Drawn By: nsn-760	